ESA Climate Change Initiative (CCI)

Climate Assessment Report (CAR)

for Climate Research Data Package No. 6 (CRDP#6)

of the Essential Climate Variable (ECV)

Greenhouse Gases (GHG)

Project: GHG-CCI+

Frédéric Chevallier [a], Julia Marshall[b]

[a] Laboratoire des Sciences du Climat et de l'Environnement (LSCE), Gif-sur-Yvette, France

[b] Institut für Physik der Atmosphäre, Deutsches Zentrum für Luft- und Raumfahrt (DLR), Oberpfaffenhofen, Germany

Change log:

Version Nr.	Date	Status	Reason for change
Version 1.2	20 March 2020	Approved (*)	User assessment for CRDP#5 XCO_2 products
Version 2.0	9 March 2021	Submitted	User assessment for CRDP#6 XCO_2 and XCH_4 products

(*) https://www.iup.uni-bremen.de/carbon_ghg/docs/GHG-CCIplus/CRDP5/GHG-CCIp_CARv5_v1.2.pdf

This document should be cited as:

Chevallier, F. and Marshall, J., Climate Assessment Report for the GHG-CCI+ project of ESA's Climate Change Initiative, pp. 59, version 2.0, 9 March 2021, 2021.

Table of content

1. Executive summary ... 4

2. User related aspects discussed in the peer-reviewed literature ... 9

3. Assessment of satellite-derived XCO_2 products ... 13

3.1. Introduction ... 13

3.2. Comparisons with forward model simulations ... 13

3.2.1. Method ... 13

3.2.2. Results ... 14

3.3. Inversion experiments with the LSCE system ... 17

3.3.1. Method ... 17

3.3.2. Global annual atmospheric growth rates ... 18

3.3.3. Maps of annual budgets ... 19

3.3.4. Annual budget time series ... 20

3.3.5. Differences with aircraft measurements ... 23

3.3.6. Conclusions ... 25

4. Assessment of satellite-derived XCH_4 data products ... 26

4.1. Introduction ... 26

4.2. Comparisons with forward model simulations ... 27

4.2.1. Method ... 27

4.2.2. Results ... 28

4.2.2.1. Overview of measurement coverage ... 28

4.2.2.2. Bias-correction based on surface-optimized fields ... 34

4.3. Methane inversion experiments with the Jena CarboScope ... 36

4.3.1. Method ... 36

4.3.2. Global mean atmospheric mixing ratio and growth rate ... 37

4.3.3. Maps of annual budgets ... 40

4.3.4. Monthly budget time series ... 42

4.3.5. Comparison with aircraft data and TCCON ... 43

4.3.6. Conclusions ... 45

Acknowledgements ... 47

References ... 48

1. Executive summary

This report describes the **assessment of the Essential Climate Variable (ECV) data products of the sixth release of the GHG-CCI Climate Research Data Package** (CRDP#6) by the Climate Research Group (CRG) of the GHG-CCI+ project (Buchwitz et al. 2015, 2017; see also GHG-CCI+ website https://climate.esa.int/en/projects/ghgs/). These products are CO_2 and CH_4 column retrievals (XCO_2 and XCH_4) from current satellite instruments:

- **CO2_OC2_FOCA:** XCO_2 from NASA's OCO-2 satellite retrieved by University of Bremen using the FOCAL algorithm (global, Jan. 2015 – May 2020, v09)
- **CO2_TAN_OCFP:** XCO_2 from China's TanSat satellite retrieved by University of Leicester using the UoL-FP (or OCFP) algorithm (2 months, v1.0)
- XCO_2 and XCH_4 from Japan's GOSAT-2 satellite (products **CO2_GO2_SRFP**, **CH4_GO2_SRFP**, **CH4_GO2_SRPR**, 9 months, v1.0.0)
- **CH4_S5P_WFMD:** XCH_4 from the European Sentinel-5-Precursor (S5P) satellite retrieved by University of Bremen using the WFM-DOAS algorithm (global, Nov. 2017 – July 2020, v1.2)

These product are (or will soon be) available via the CCI Open Data Portal (https://climate.esa.int/en/odp/#/dashboard).

Climate researchers may find interest in these products for various reasons like evaluating climate models, estimating the uncertain parameters of these climate models, studying the variability of CO_2 and CH_4 in the atmosphere, studying wildfire or fossil fuel emission plumes, or quantifying the surface fluxes of these gases.

CRDP#6 is the second release of products from the GHG-CCI+ project, which started in March 2020.

Datasets CRDP#1 to CRDP#4 have been generated and released by the GHG-CCI pre-cursor project (2010 - 2018). These products are CO_2 and CH_4 products from SCIAMACHY/ENVISAT, MIPAS/ENVISAT, GOSAT, AIRS and IASI. The XCO_2 and XCH_4 and IASI products are now generated operationally via the Copernicus Climate Change Service (C3S, https://climate.copernicus.eu/) and are available via the Copernicus Climate Data Store (CDS, https://cds.climate.copernicus.eu/).

By producing retrievals of the CO_2 and CH_4 columns for these satellites and others, CRDP has given a **unique**, though heterogeneous, **climate record from space covering now more than fifteen years** of the two major greenhouse gases of anthropogenic origin. **This length opens the possibility to characterize emission trends, as was already demonstrated by a series of CRDP-based studies for CH_4** (Bergamaschi et al. 2013) **and for CO_2** (Ross et al. 2013, Schneising et al. 2013a, 2013b, Reuter et al. 2014b, Detmers et al. 2015).

The pioneering character of these new climate records is deliberately acknowledged through the use of an ensemble of retrieval product covering several sensors and multiple retrieval algorithms (EMMA). **This ensemble approach allows a more comprehensive assessment of the product uncertainty than just the typical uncertainty characterisation of each product through internal uncertainty propagation**. Reuter et al. (2013, 2014a, 2020) well illustrated this capability.

The CRDP data sets, together with satellite retrievals made outside Europe, has already served to **quantify regional carbon budgets** (e.g., Basu et al. 2013, Bergamaschi et al. 2013, Fraser et al. 2013, Monteil et al. 2013, Cressot et al. 2013) and more specifically (for CO_2) Canada and Siberian forests (Schneising et al. 2011), Eurasia (Guerlet et al. 2013a), Tropical Asia (Basu et al. 2014), Amazonia (Parazoo et al. 2013) and Europe (Reuter et al. 2014a). However, for CO_2, there remains considerable discrepancies with bottom up estimates or inversions based on atmospheric in-situ observations (Chevallier et al. 2014a, 2019, Feng et al. 2016a, Reuter et al. 2016c). These discrepancies were also highlighted in the first five releases of the CAR (Chevallier et al. 2013, 2015, 2016, 2017, 2020). For CH_4 it has been clearly demonstrated that the SCIAMACHY retrievals and the GOSAT retrievals provide important information on regional methane emissions (e.g., Bergamaschi et al. 2013, Fraser et al. 2013, Alexe et al. 2015).

Each application of the CRDP has specific user requirements and it is not possible to exhaustively cover them in the CRG. Instead, the CRG has focussed on global source-sink inversion from several viewpoints.

For CO_2, the study has been restricted to the product in CRDP#6 that covers the whole globe and several years: CO2_OC2_FOCA which has been retrieved from OCO-2 over both land and ocean. The starting point of this report is the comparison between this product with the independent CAMS v20r1 transport model simulation (with surface fluxes inferred through inversion of high precision measurements of atmospheric CO_2 in situ samples). The satellite retrievals fit the independent CAMS simulation over land and ocean within 2.0 ppm RMS. Improved statistics are obtained when comparing NASA's ACOS OCO-2 retrievals, version 10, with the CAMS simulation over land as over ocean. This confirms that the individual ACOS retrievals have better precision than the CO2_OC2_FOCA ones, as already reported in the respective retrieval data files.

The assimilation of the CO2_OC2_FOCA product in the LSCE global inversion system infers CO_2 surface fluxes that are very different from those obtained by the assimilation of surface air-sample measurements. The CO2_OC2_FOCA-driven CO_2 surface fluxes appear to be less credible because (i) the inferred spatial distribution of the ocean outgassing regions is inconsistent with current knowledge of the marine biogeochemistry obtained from sea surface CO_2 partial pressure measurements, (ii) the inferred atmospheric growth rates for years 2017 and 2019 are notably different from the one seen at marine background stations, and (iii) the biases with aircraft data in the free troposphere are larger than when assimilation surface air-sample measurements and show a dependency on latitude. In contrast, the ACOS-driven CO_2 surface fluxes (ACOS being restricted to land retrievals here) seem to perform better than the CO2_OC2_FOCA-driven fluxes and even show comparable (marginally larger) difference statistics to aircraft measurements in the free troposphere

in output to the transport model compared to surface-air-sample-driven fluxes. This result demonstrates that there is no fundamental limitation to atmospheric inverse modelling (e.g., in the realism of the transport model or in the modelled error statistics) when assimilating satellite XCO_2 retrievals. It has also motivated the distribution of the ACOS-driven CO_2 surface fluxes as part of the official CAMS inversion products (http://www.copernicus-atmosphere.eu/).

The various tests performed do not allow us to identify the distinctive asset of ACOS vs. CO2_OC2_FOCA in our system: either the data density, the data precision, the data trueness, the accuracy of the auxiliary data (averaging kernels) or a combination of these qualities at once. Detailed sensitivity tests could be performed for this. CO2_OC2_FOCA's distinct advantage compared to ACOS is its representation of multiple scattering effects in the radiative transfer in a form that is not costlier than absorption. In preparation for the Copernicus CO_2 Monitoring Mission that will provide even larger amount of data than OCO-2, CO2_OC2_FOCA represents an important achievement. In this context and resources permitting, it would be important to document its performance with more detail in order to help prioritize future developments.

For CH_4, the only data product in CRDP#6 that covers the whole globe more than one full year is CH4_S5P_WFMD. In order to expand the scope of this assessment, the operational S5P retrieval using the RemoTeC algorithm (hierafter referred to as CH4_S5P_SRON) has been included in the assessment, as well as the pre-operational RemoTeC product based on Lorente et al. (2021), referred to as CH4_S5P_SRONt. Furthermore, some initial comparison of the GOSAT-2 retrievals (CH4_GO2_SRFP and CH4_GO2_SRPR) have been included as well. While these retrievals are only currently available for nine months, too short a period to perform global inversions, this first impression already provides some user feedback.

The comparison beging by comparing the XCH_4 products to an inversion optimized using measurements from 31 flask measurement sites around the world. This is a rather limited dataset, but it is what is available over the time period in question. In fact, the most recent satellite retrievals are available considerably earlier than in-situ measurements, which is a limitation when assessing retrievals less than a year after the measurement time.

The comparison of the surface-optimized concentration fields with the satellite products shows a systematic offset with a latitudinal dependence. This is likely largely due to errors in the transport model with respect to poorly represented tropopause height and stratospheric gradients. In order to not map this transport error onto the resultant fluxes, a 2^{nd} order polynomial correction is applied. Assessing the shape of this correction shows that the latitudinal gradients of the CH4_S5P_WFMD and CH4_S5P_SRONt retrievals from the commissioning phase (prior to April 2018) are rather different than the same months in following years. Encouragingly, the derived bias corrections between retrievals over ocean and land for CH4_S5P_WFMD are essentially identical, showing no evidence of a land-sea bias. The derived bias corrections for the GOSAT-2 products are also similar to that for CH4_S5P_WFMD as well as to each other (SRFP and SRPR). Some larger differences are seen for the CH4_S5P_SRON retrieval, particularly at higher latitudes, suggesting some problems in the retrieval, potentially related to snow cover. While some of the high- and low-albedo errors were

corrected in the pre-operational retrieval CH4_S5P_SRONt, this product shows anomalously low values for some regions for days in 2020, particularly in April and May.This type of spatially and temporally consistent systematic error has particularly severe impacts in the context of inverse modelling.

Inversions were carried out using CH4_S5P_WFMD, CH4_S5P_SRON, and CH4_S5P_SRONt from January 2018 through June 2020, although there are CH4_S5P_WFMD and CH4_S5P_SRONt retrievals available as early as November 2017 and the operational retrieval extends already into 2021. This period was chosen due to the limited availability of surface data beyond mid-2020 and the lower quality and gaps in the satellite retrievals during the commissioning phase.

The assimilation of the S5P retrievals in the Jena-CarboScope global inversion system results in methane fluxes that are substantially different in spatial distribution from those obtained by the assimilation of surface air-sample measurements, but in general agreement with each other. The resultant global mean near-surface concentrations show comparable variability to and high correlation with global mean concentration estimates from NOAA and WDCGG, based on in-situ measurements. The time period is quite short, making it difficult to make robust conclusions about the derived global growth rates, but also here the results between the different inversions are statistically consistent with one another.

Many of the inferred flux increments appear plausible, as they are related to areas with considerable uncertainty in the surface fluxes and with a poor data coverage in the surface-based measurement network. Both the CH4_S5P_WFMD and CH4_S5P_SRON retrievals show a decrease in methane fluxes over much of China and India (compared to both the prior and the surface-based inversion), and an increase in emissions in the Middle East and Central Asia. Reduced methane emissions are inferred for both Boreal Eurasia and North America, coupled with increased emissions over the Eurasian Arctic.

When seen in the annual mean and considering driving processes, these fluxes could be plausible, but when looking at the monthly timeseries of the fluxes aggregated onto TransCom regions, the temporal variability is extreme. The satellite-based inversions suggest an unrealistically large seasonal cycle in both Europe and Temperate North America, possibly as a dipole to the small (large) seasonal cycle inferred for Boreal North America (Eurasia). While both the CH4_S5P_WFMD and CH4_S5P_SRON inversions exhibited these problems, they were slightly more severe in the CH4_S5P_SRON inversion. In the assessment of global mean near-surface concentration, the CH4_S5P_WFMD inversion was also better correlated with both the surface-based inversion and the NOAA and WDCGG estimates, suggesting a better consistency with the surface measurements.

The resultant concentration fields were compared to independent measurements, namely aircraft profiles and total column measurements from the TCCON network of surface-based Fourier Transform Spectrometers. These results show that that satellite-based inversions agree better with TCCON than does the surface-based inversion, while the

Some of the unphysical or unlikely flux results can be ameliorated by changing the settings of the inversion system: e.g. increasing temporal and spatial correlation lengths, inflating the estimated model-data mismatch error, or giving more weight to the prior. Simultaneously assimilating surface-based and satellite measurments may also help to anchor the model to a more physical result. For the scientific interpretation of the satellite retrievals, this will be required. The assessment presented here simply draws attention to the current retrievals are not (yet) fully consistent with our knowledge of the surface fluxes based on surface measurements.

2. User related aspects discussed in the peer-reviewed literature

The GHG-CCI project primarily aims at bringing new knowledge about the sources and sinks of CO_2 and CH_4 based on satellite-derived data products. Since the start of Phase 1 of the GHG-CCI pre-cursor project in 2010, this aspect has been addressed in a series of publications, which are shortly summarised in the following. They usefully provide the background for the new studies that have been performed specifically for this report and that will be described next. For a full list of publications see "Project publications" on https://climate.esa.int/en/projects/ghgs/publications/.

We start with the publications related to natural CO_2 fluxes.

- Using global GOSAT XCO_2 retrievals, Basu et al. (2013) presented first global CO_2 surface flux inverse modelling results for various regions. Their analysis suggested a reduced global land sink and a shift of the carbon uptake from the tropics to the extra-tropics. In particular, their results suggested that Europe is a stronger carbon sink than expected, but this feature was not further discussed in this paper.
- Chevallier et al. (2014a) analysed an ensemble of global inversion results assimilating two GOSAT XCO_2 retrieval products. They found hemispheric and regional differences in posterior flux estimates that are beyond 1 sigma uncertainties. They too found a significantly larger European carbon sink or a larger North African emission than expected. They concluded to the existence of significant flaws in all main components of the inversions: the transport model, the prior error statistics and the retrievals.
- Houweling et al. (2015) presented the outcome of a large inverse modelling intercomparison experiment on the use of GOSAT retrievals. The ensemble of results confirmed the large latitudinal shift in carbon uptake, but they showed that the reduced gradient degrades the agreement with background aircraft and surface measurements.
- Reuter et al. (2014a) investigated the European carbon sink further with another ensemble of GOSAT XCO_2 products, a SCIAMACHY XCO_2 product and a new inversion method which is less sensitive to some of the issues discussed in Chevallier et al. (2014a). Reuter et al. (2014a) only used satellite XCO_2 retrievals over Europe to rule out that non-European satellite data adversely influence the European results and they also only used short-term (days) transport modelling to avoid long-range transport errors. Based on an extensive analysis they concluded: "We show that the satellite-derived European terrestrial carbon sink is indeed much larger (1.02 ± 0.30 GtC/year in 2010) than previously expected". The value they derived is significantly larger compared to bottom-up estimates (not based on atmospheric measurements) of 0.235 ± 0.05 GtC/year for 2001-2004 (Schulze et al, 2009).
- The findings of Reuter et al. (2014a) stimulated additional research (Feng et al. 2016a, Reuter et al. 2016c).
- Detmers et al. (2015) analyzed GOSAT XCO_2 retrievals to detect and quantify anomalously large carbon uptake in Australia during a strong La Niña episode.
- For flux inversions not only the retrieved greenhouse gas values are relevant but also their error statistics, in particular the reported uncertainties. Chevallier and O'Dell (2013) analyzed this aspect in the context of CO_2 flux inversions using GOSAT XCO_2 retrievals. For CH_4, Cressot et al. (2013, 2016) studied the uncertainty of flux inversions assimilating SCIAMACHY, GOSAT or IASI XCH_4 retrievals.
- Focussing on Canadian and Siberian boreal forests, Schneising et al. (2011) computed longitudinal XCO_2 gradients from SCIAMACHY XCO_2 retrievals during the vegetation growing season over Canadian and Siberian boreal forests and compared the gradients with outputs from NOAA's CO_2 assimilation system CarbonTracker (Peters et al. 2007). They found good agreement for the total

boreal region and for inter-annual variations. For the individual regions, however, they found systematic differences suggesting a stronger Canadian boreal forest growing season CO_2 uptake and a weaker Siberian forest uptake compared to CarbonTracker.

- Focussing on hemispheric data and on carbon-climate feedbacks, Schneising et al. (2014a) used SCIAMACHY XCO_2 to study aspects related to the terrestrial carbon sink by looking at co-variations of XCO_2 growth rates and seasonal cycle amplitudes with near-surface temperature. They found XCO_2 growth rate changes of 1.25 ± 0.32 ppm/year/K (approximately 2.7 ± 0.7 GtC/year/K; indicating less carbon uptake in warmer years, i.e., a positive carbon-climate feedback) for the Northern Hemisphere in good agreement with CarbonTracker.
- Reuter et al. (2013) computed CO_2 seasonal cycle amplitudes using various satellite XCO_2 data products (using GHG-CCI products but also GOSAT XCO_2 products generated in Japan at NIES (Yoshida et al. 2013, Oshchepkov et al. 2013) and the NASA ACOS product (O'Dell et al. 2012) and compared the amplitudes with TCCON and CarbonTracker. They found that the satellite products typically agree well with TCCON but they found significantly lower amplitudes for CarbonTracker suggesting that CarbonTracker underestimates the CO_2 seasonal cycle amplitude by approx. 1.5 ± 0.5 ppm (see also Buchwitz et al., 2015, for a discussion of these findings).
- Lindquist et al. (2015) compared satellite XCO_2 retrievals, surface XCO_2 retrievals and atmospheric model simulations in terms of XCO_2 seasonal cycle. They found that the satellite retrieval algorithms performed qualitatively similarly but showed notable scatter at most validation sites. None of the tested algorithm clearly outperformed another. They showed that the XCO_2 seasonal cycle depends on longitude especially at the mid-latitudes, which was only partially shown by the models. They also found that model-to-model differences could be larger than GOSAT-to-model differences.
- Guerlet et al. (2013a) analyzed GOSAT XCO_2 retrievals focusing on the Northern Hemisphere. They identified a reduced carbon uptake in the summer of 2010 and found that this is most likely due to the heat wave in Eurasia driving biospheric fluxes and fire emissions. Using a joint inversion of GOSAT and surface data, they estimated an integrated biospheric and fire emission anomaly in April–September of 0.89 ± 0.20 PgC over Eurasia. They found that inversions of surface measurements alone fail to replicate the observed XCO_2 inter-annual variability (IAV) and underestimate emission IAV over Eurasia. They highlighted the value of GOSAT XCO_2 in constraining the response of land-atmosphere exchange of CO_2 to climate events.
- Basu et al. (2014) studied seasonal variation of CO_2 fluxes during 2009-2011 over Tropical Asia using GOSAT, CONTRAIL and IASI data. They found an enhanced source for 2010 and concluded that this is likely due to biosphere response to above-average temperatures in 2010 and unlikely due to biomass burning emissions.
- Parazoo et al. (2013) used GOSAT XCO_2 and solar induced chlorophyll fluorescence (SIF) retrievals to better understand the carbon balance of southern Amazonia.
- Ross et al. (2013) used GOSAT data to obtain information on wildfire CH_4:CO_2 emission ratios.

Despite the fact that none of the existing satellite missions has been optimized to obtain information on anthropogenic CO_2 emissions, this important aspect has been addressed in several recent publications using existing satellite XCO_2 products.

- Schneising et al. (2013) presented an assessment of the satellite data over major anthropogenic CO_2 source regions. They used a multi-year SCIAMACHY XCO_2 data set and compared the regional XCO_2 enhancements and trends with the emission inventory EDGAR v4.2 (Olivier et al. 2012). They found no significant trend for the Rhine-Ruhr area in central Europe and the US East Coast but a significant

increasing trend for the Yangtze River Delta in China of about 13 ± 8%/year, in agreement with EDGAR (10 ± 1%/year).

- Reuter et al. (2014b) studied co-located SCIAMACHY XCO_2 and NO_2 retrievals over major anthropogenic source regions. For East Asia they found increasing emissions of NO_x (+5.8%/year) and CO_2 (+9.8%/year), i.e., decreasing emissions of NO_x relative to CO_2 indicating that the recently installed and renewed technology in East Asia, such as power plants and transportation, is cleaner in terms of NO_x emissions than the old infrastructure, and roughly matches relative emission levels in North America and Europe.

A series of studies also addressed methane emissions.

- SCIAMACHY data have already been extensively used to improve our knowledge on regional methane emissions prior to the start of the GHG-CCI project (e.g., Bergamaschi et al. 2009). A more recent research focus was to shed light on the unexpected renewed atmospheric methane increase during 2007 and later years using ground-based and satellite data (e.g., Rigby et al. 2008, Dlugokencky et al. 2009, Bergamaschi et al. 2009, 2013, Schneising et al. 2011, Frankenberg et al. 2011, Sussmann et al. 2012, Crevoisier et al. 2013). Based on an analysis of SCIAMACHY year 2003-2009 retrievals an increase of 7-9 ppb/year (0.4-0.5%/year) has been found with the largest increases in the tropics and northern mid latitudes (Schneising et al. 2011) but a particular region responsible for the increase has not been identified (Schneising et al. 2011; Frankenberg et al. 2011). Bergamaschi et al. (2013) used SCIAMACHY retrievals and NOAA surface data for 2003-2010 and inverse modelling in order to attribute the observed increase of atmospheric concentrations to changes in emissions. They concluded that most of this increase is due to emissions in the Tropics and the mid-latitudes of the northern hemisphere, while no significant trend was derived for Arctic latitudes. The increase is mainly attributed to anthropogenic sources, superimposed with significant inter-annual variations of emissions from wetlands and biomass burning.
- Methane emissions have also been obtained from GOSAT, as presented in a number of publications as shown in, e.g., Fraser et al. (2013, 2014), Monteil et al. (2013), Cressot et al. (2014), Alexe et al. (2015), Turner et al. (2015) and Pandey et al. (2016). Note that for these studies often CH_4 retrievals from several satellites have been used (as well as NOAA data), e.g., Monteil et al. (2013), and Alexe et al. (2015) used SCIAMACHY and GOSAT retrievals and Cressot el al. (2014, 2016) used GOSAT, SCIAMACHY and IASI. Alexe et al. (2015) showed that the different satellite products resulted in relatively consistent spatial flux adjustment patterns, particularly across equatorial Africa and North America. Over North America, the satellite inversions result in a significant redistribution of emissions from North-East to South-Central USA, most likely due to natural gas production facilities.
- Several publications focused on (relatively localized) methane sources in the United States: For example, Schneising et al. (2014b) analyzed SCIAMACHY data over major US "fracking" areas and quantified methane emissions and leakage rates. For two of the fastest growing production regions in the US, the Bakken and Eagle Ford formations, they estimated that emissions increased by 990 ± 650 $ktCH_4$/year and 530 ± 330 $ktCH_4$/year between the periods 2006–2008 and 2009–2011. Relative to the respective increases in oil and gas production, these emission estimates correspond to leakages of 10.1% ± 7.3% and 9.1% ± 6.2% in terms of energy content, calling immediate climate benefit into question and indicating that current inventories likely underestimate the fugitive emissions from Bakken and Eagle Ford. Others also used SCIAMACHY data over the US to identify and quantify localized anthropogenic methane emission sources (Kort et al. 2014, Wecht et al. 2014). Last, Turner et al. (2015) used GOSAT retrievals within a meso-scale inversion system for the US.

The SCIAMACHY XCH_4 retrievals have also been used to improve chemistry-climate models (Shindell et al. 2013, Hayman et al. 2014).

3. Assessment of satellite-derived XCO_2 products

3.1. Introduction

Given nearly a decade (since Basu et al., 2013, see Section 2) of global inverse modelling studies assimilating real XCO_2 retrievals, extended to 1.5 decades (Chevallier et al., 2005) in the case of partial column CO_2 retrievals, the current interest in XCO_2 products for global inverse modelling is about multi-year global products. This has not been always the case (Chevallier et al, 2011). The first four GHG-CCI Climate Research Data Packages fulfilled this ambition with SCIAMACHY and TANSO retrievals.

The 6th GHG-CCI+ Climate Research Data Package (CRDP#6, http://cci.esa.int/ghg#data) includes three CO_2 products:

- CO2_OC2_FOCA: retrieved from OCO-2 using University of Bremen's FOCAL algorithm
- CO2_TAN_OCFP: retrieved from TanSat using University of Leicester's UoL-FP (or OCFP) algorithm
- CO2_GO2_SRFP: retrieved from GOSAT-2 using SRON's RemoTeC (or SRFP) algorithm

At the scale of the GHG-CCI+ project, the goal for all three is to make multi-year global products available, but currently only the first one, CO2_OC2_FOCA, fulfils this criterion. It is evaluated in this chapter within a forward and inverse modelling framework, and in comparison with version 10 of the official bias-corrected XCO_2 retrievals made by the NASA Atmospheric CO_2 Observations from Space (ACOS) algorithm described by Osterman et al. (2020). The motivation behind using ACOS here lies in its prominent use in the science community.

The evaluated product from CRDP is summarized in Table 1 below. The official bias-corrected product has been processed by LSCE.

Product ID	Instrument	Algorithm	Data provider	Reference	Period available	Evaluators (sections)
CO2_OC2_FOCA	OCO-2	FOCAL, v9	IUP, Univ. Bremen	Reuter et al., 2017a, 2017b	01/2015-05/2020	LSCE (3.2, 3.3)

Table 1. XCO_2 products evaluated in this report.

3.2. Comparisons with forward model simulations

3.2.1. Method

In this section, we compare CO2_OC2_FOCA with a forward simulation of the LMDZ transport model (Hourdin et al. 2013) nudged to the ERA5 reanalysis and using surface fluxes from a classical atmospheric inversion that assimilated surface air-sample measurements. Our forward simulation

comes from the CAMS CO_2 inversion product driven by surface air-sample measurements (version 20r1, https://atmosphere.copernicus.eu/), an earlier version of which was described by Chevallier et al. (2010a). It uses the LMDZ transport model with a recent configuration of the model physics (Remaud et al., 2018). In space, the model is discretized into 39 vertical layers, 3.75 longitude degrees and 1.9 latitude degrees. Compared to ground retrievals from the Total Carbon Column Observing Network (TCCON, Wunch et al., 2011) at non-urban sites for the 2004-2020 period, absolute biases are less than 1 ppm at all sites, and the standard deviation is usually about 1 ppm, exceptionally reaching 2.2 ppm at the Zugspitze mountain site (Chevallier, 2020). The standard deviation of the model-minus-TCCON differences, resulting from both model and retrieval errors, is therefore smaller than the reported FOCAL Bayesian uncertainty (1 σ ~ 1.2 ppm) but also larger than the reported ACOS Bayesian uncertainty (1 σ ~ 0.5 ppm).

When comparing model and XCO_2 retrievals, we account for the prior profiles and the averaging kernels of each individual retrieval. The OCO-2 retrievals have much higher spatial resolution than the global LMDZ model, by several orders of magnitude, but in this section we use them individually, without any averaging, in contrast to the next section about inverse modelling. For both OCO-2 products, we compute the statistics of their difference with the model simulation in three latitude bands: the latitudes north of 25°N, the latitudes south of 25°S and the latitudes between 25°S and 25°N. The CO2_OC2_FOCA data files do not make the distinction between land and ocean retrievals and we do not attempt at getting this information from some other source using the latitude and longitude coordinates. Since the sounding land type is reported in the ACOS product (variable *land_water_indicator*), we stratify the ACOS results per geotype. All statistics are for the period between January 2015 and May 2020.

3.2.2. Results

Multiyear-results are summarized in Figure 1. Since we have no way to distinguish between random errors and systematic ones in the retrieval products and in the forward simulation, and following the usual practice (e.g., Desroziers et al. 2005), we use the root mean square (RMS) to characterize the statistics of the model-minus-observation departures, rather than the standard deviation.

The number of data feeding the statistics (the pink bars in Figure 1) varies with the screening performed in the corresponding retrieval algorithm: there is 3.6 times more ACOS data than CO2_OC2_FOCA data in the 65-month study period. The RMS departures (the orange disks in Figure 1) are between 1.3 and 2.0 ppm for CO2_OC2_FOCA and are less than 1.3 ppm for ACOS. They seem to confirm the greater uncertainty of CO2_OC2_FOCA products compared to ACOS products, that was already suggested by the difference in reported Bayesian uncertainty (see Section 3.2.1).

The precision and bias of CO2_OC2_FOCA has been assessed independently (Table 4-1 in Product Validation and Intercomparison Report, PVIR, Buchwitz et al. 2021) based on TCCON observations. The scatter of the retrieval misfits to TCCON is overall similar to the scatter of the retrieval misfits to the model presented here.

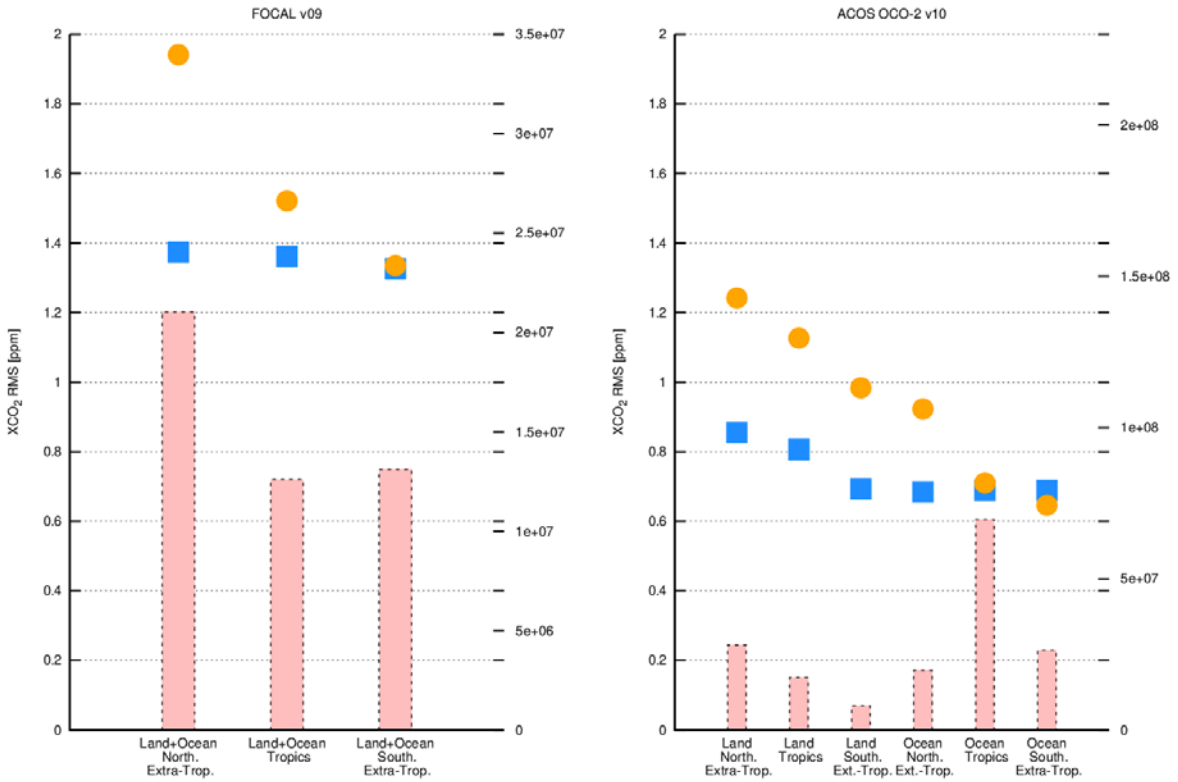

Figure 1. The orange disks show the Root Mean Squared values (RMS) of the misfits between the three XCO_2 products indicated in the plot titles and the reference CAMS surface-driven simulation for the period between January 2015 and May 2020. The blue squares represent the root mean square of the sum of the CAMS simulation error variances and of the retrieval error variances. The globe is divided into three latitude bands. For ACOS, as in the corresponding data files, land and ocean are separated. The number of data included in the statistics is reported as vertical pink bars.

We now compare the RMS values of Figure 1 with the "bottom-up" quadratic sum of their components (the blue squares in Figure 1): the retrieval Bayesian uncertainty and the model uncertainty. We refer to Chevallier and O'Dell (2013) for more background about the underlying principles. We take the retrieval Bayesian uncertainty directly from the product data files: as said above, the reported 1 σ is about 1.2 and 0.5 ppm, respectively for CO2_OC2_FOCA and ACOS. Following the approach described in Chevallier and O'Dell (2003), we estimate the 1 σ model uncertainty to be about 0.6 ppm, a value which is consistent with the model-minus-TCCON differences seen at most non-urban sites, given TCCON retrieval uncertainty (Chevallier, 2020).

Figure 1 shows that the bottom-up error budget is underestimated for both OCO-2 products, except in the southern hemisphere for CO2_OC2_FOCA and in the tropical and southern oceans for ACOS. In the case of CO2_OC2_FOCA, the underestimation north of 25°N likely reflects underestimated precision, because the retrieval uncertainty already dominates the error budget. The PVIR came to a similar conclusion by comparing CO2_OC2_FOCA to TCCON (Table 4-2 of Buchwitz et al. 2021).

The reason for the underestimation is less clear for ACOS because the smaller RMS and the much smaller reported retrieval uncertainty suggests an even balance between model uncertainty and retrieval uncertainty, that both could be a little underestimated, and also leaves room for a noticeable impact of retrieval systematic errors in the RMS.

3.3. Inversion experiments with the LSCE system

3.3.1. Method

In this section, we go one step further in the evaluation of CO2_OC2_FOCA with the LSCE system by interpreting the model-data misfits shown in Section 3.2 in terms of surface fluxes. The satellite data are assimilated alone, without combining them with other observations, in order to focus on their own signals. In order to avoid numerical artifacts caused by the much higher spatial resolution of the retrievals than the model, we follow Crowell et al. (2019) by aggregating the OCO-2 retrievals from CO2_OC2_FOCA and ACOS in 10-second intervals, that roughly correspond to boxes of 67×10 km^2, a surface area which is still much smaller than the individual model grid boxes of 3.75° × 1.9°. We use CO2_OC2_FOCA and ACOS candidly, i.e. without modifying the retrieval values and their associated uncertainty in input to the 10-s binning algorithm described in Section 3.2.1. However, if several 10-s-binned retrievals of a same orbit fall within the same model grid box, we inflate the variance of the retrieval errors by the number of concerned 10-s-binned retrievals, in order to avoid likely local error correlations (at least from the transport model). As in the previous section, we use the retrieval averaging kernels and prior profiles when assimilating them. Processing the full multi-year series of CO2_OC2_FOCA within the inverse system required about one month of computation on 10 parallel CPU cores on the LSCE cluster.

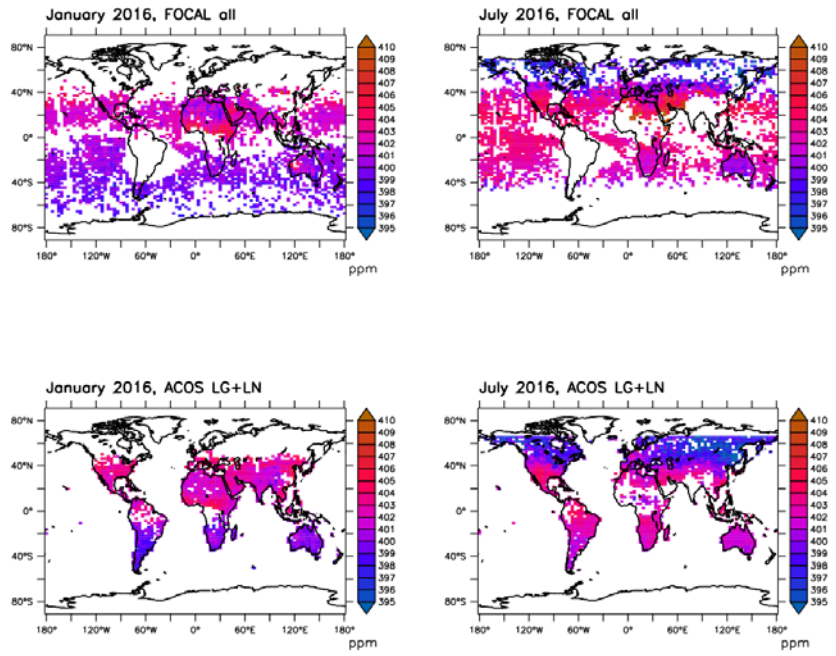

Figure 2. Average of the retrievals (as they are assimilated here) in each model grid box for January and July 2016. CO2_OC2_FOCA (both lands and oceans) and ACOS (land only) are shown in the top and bottom rows, respectively.

The fluxes inferred from CO2_OC2_FOCA are compared to two benchmark inversion: the CAMS official inversion products v20r1 (used in Section 3.2) that exclusively assimilated 156 sites of surface air-sample measurements from the Global Atmosphere Watch programme, and the CAMS official inversion product FT20r2 that exclusively assimilated the ACOS OCO-2 retrievals over land. Ocean glint retrievals were not assimilated in FT20r2 because of likely systematic errors (Chevallier et al., 2019), but such a selection is not done for CO2_OC2_FOCA here in the absence of similar evidence. Still, many more ACOS retrievals are assimilated than CO2_OC2_FOCA ones in the respective inversions (see Figure 1) due to much stricter filter criteria that leave large regions unobserved or poorly observed during full months in the latter (Figure 2).

The inversion system works at the grid-point weekly scale and generates a large volume of data. The present comparison focuses on a few key quantities: (i) the global annual growth rate that is well known from the NOAA marine surface data (Conway et al. 1994, http://www.esrl.noaa.gov/gmd/ccgg/trends/global.html), (ii) the grid-point annual-total fluxes, (iii) the regional annual CO_2 budgets.

3.3.2. Global annual atmospheric growth rates

Figure 3 shows the time series of the global annual growth rates from NOAA, from the CAMS inversions and from CO2_OC2_FOCA. We use a conversion factor of 2.086 GtC·ppm^{-1} from Prather (2012). Note that the NOAA estimate and the surface-driven CAMS one are not independent since the surface-driven CAMS inversion assimilates the individual NOAA measurements. Their difference has a standard deviation of 0.16 ppm and a bias of -0.02 ppm (based on 41 yearly values). The statistics estimate for the OCO-2-driven CAMS inversion is of -0.06±0.11 ppm (the estimate is based on 5 annual values). The differences between the growth rate from the CO2_OC2_FOCA inversion and the NOAA estimate have a bias twice as small but a scatter three times as large: a bias of -0.03 ppm and a standard deviation of 0.27 ppm (based on 5 values). Note that the quality of the growth rate in the CO2_OC2_FOCA retrievals themselves may be much better, but since they do not cover the full globe all the time, the inversion system, informed by the transport model (hard constraint), may generate very different XCO_2 between the retrievals, for instance to fit small spurious retrieval signals.

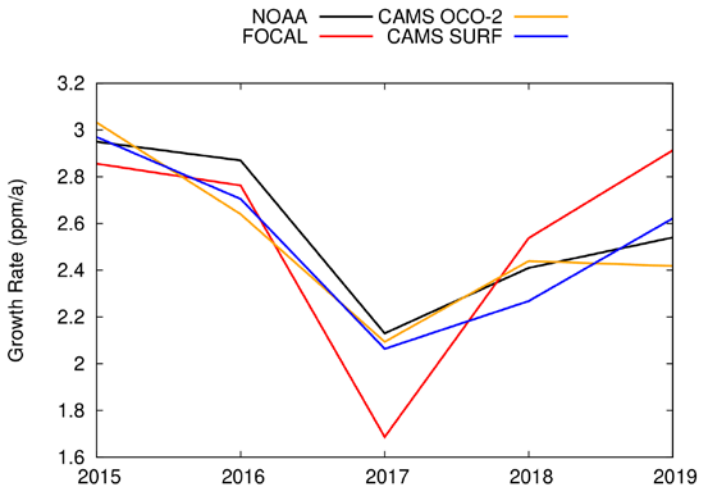

Figure 3. Global annual atmospheric growth rate from NOAA (ftp://aftp.cmdl.noaa.gov/products/trends/co2/co2_gr_gl.txt, accessed 8 February 2021) between years 2015 and 2019, from the 2 official CAMS inversions and from CO2_OC2_FOCA.

3.3.3. Maps of annual budgets

Figure 4 displays the maps of the inferred annual budgets of natural CO_2 for the year 2015. As shown already by Chevallier et al. (2019), the two CAMS inversions have comparable flux patterns in the northern extra-Tropics, but the ACOS-driven inversion has more spatial gradients than the surface-driven one in the Tropical lands where the surface measurement network is particularly sparse. The CO2_OC2_FOCA inversion has even larger gradients there (Australia excepted), but also in the northern extra-Tropics. The colour bar has actually not been adapted to their variability. Surprisingly, the spatial patterns (irrespective of their amplitude) are similar between the two satellite-driven inversions over land. Over the ocean, the two CAMS inversions are close to each other, but CO2_OC2_FOCA dramatically shifts the location of the outgassing regions.

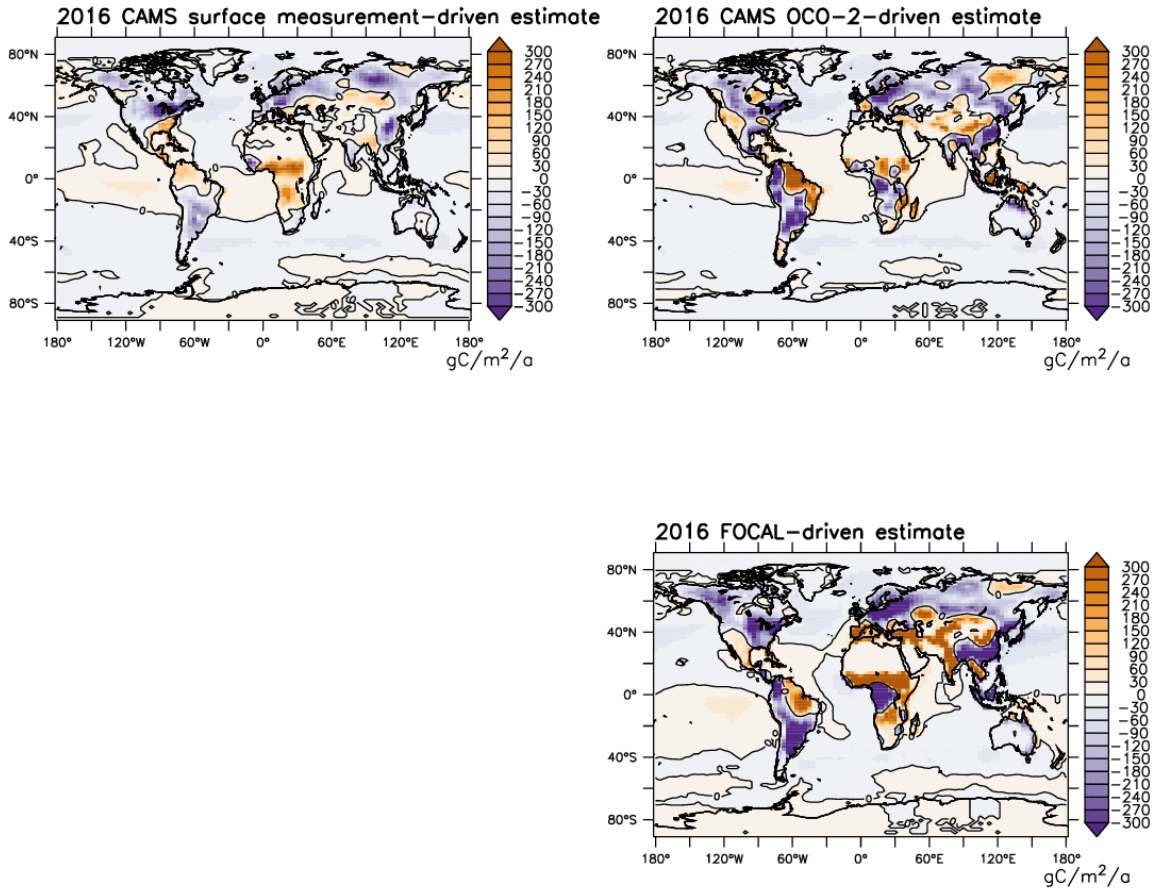

Figure 4. Grid-point budget of the natural CO_2 fluxes for the year 2016 and for the two CAMS inversions and for the CO2_OC2_FOCA product. In the sign convention, positive fluxes correspond to a net carbon source into the atmosphere.

3.3.4. Annual budget time series

The time series of the annual natural carbon budgets at several very broad scales are displayed in Figure 5 for the period between 2004 and 2019: the globe, the northern or southern extra-Tropics, and the Tropics with lands and oceans either separated or combined. At the global scale (top row), the curves reflect the growth rate curves of Figure 3, but without the fossil fuel and cement flux component. The three inversions locate the land sink mostly in the northern extra-Tropics, eventhough a large year-to-year variability is seen in the Tropics. The southern extra-Tropical lands (that represent a relatively small surface area) are close to neutral each year. The ACOS inversion is well within the 1σ uncertainty of the surface inversion (except for the last year in the southern extra-Tropical lands), which is less the case for the CO2_OC2_FOCA inversion. Over the oceans, the two CAMS inversions agree less with each other, relative to the 1σ envelope, but the CO2_OC2_FOCA inversion is even further away. The Southern Ocean sink, in particular, is found twice as small when assimilating the CO2_OC2_FOCA retrievals vs. the surface measurements.

Detailed results at the scale of the 22 regions of the TransCom 3 experiment (Gurney et al., 2002, Figure 6) are shown in Figure 7 (11 regions over land) and Figure 8 (11 regions over the ocean). The 22 regions together tile the whole globe, apart from the polar ice caps. The two figures show results consistent with the above results, with the CAMS inversions close to each other in most regions and the CO2_OC2_FOCA inversion further away in terms of 5-year average (less so in terms of variability).

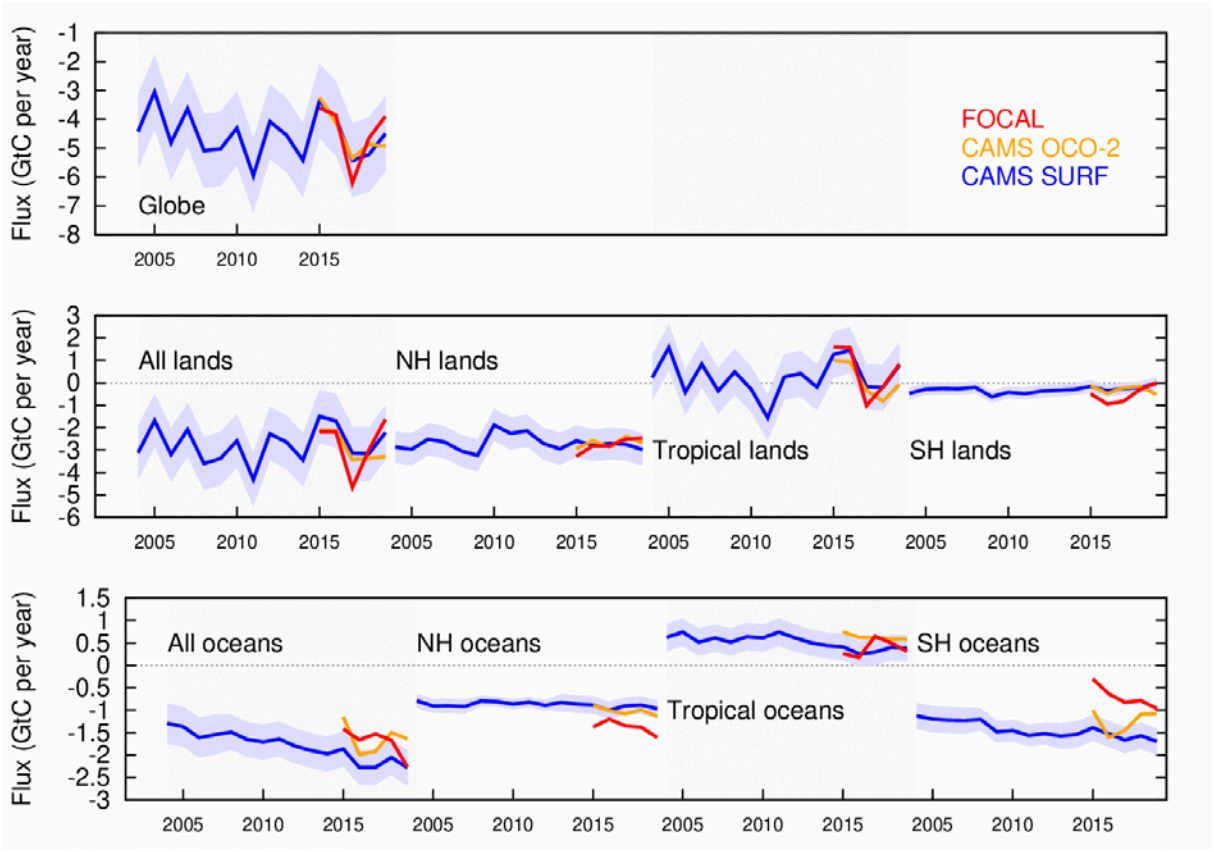

Figure 5. Inferred natural CO_2 annual flux (without fossil fuel emissions) averaged over the globe or over all lands or oceans. In the case of lands and oceans, three broad latitude bands are also defined: northern extra-Tropics (north of 25°N), Tropics (within 25° of the Equator), and southern extra-Tropics (south of 25°S). The blue curve corresponds to the surface-driven CAMS product with its 1-sigma Bayesian uncertainty. In the sign convention, positive fluxes correspond to a net carbon source into the atmosphere.

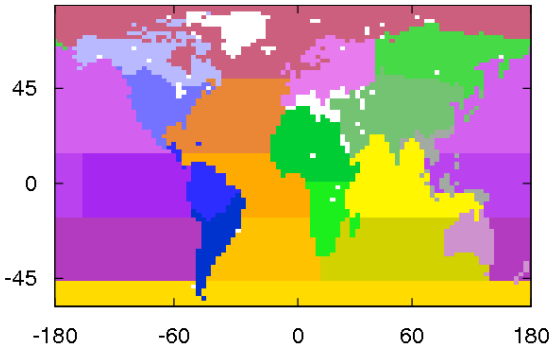

Figure 6. Transcom regions from Gurney et al. (2002).

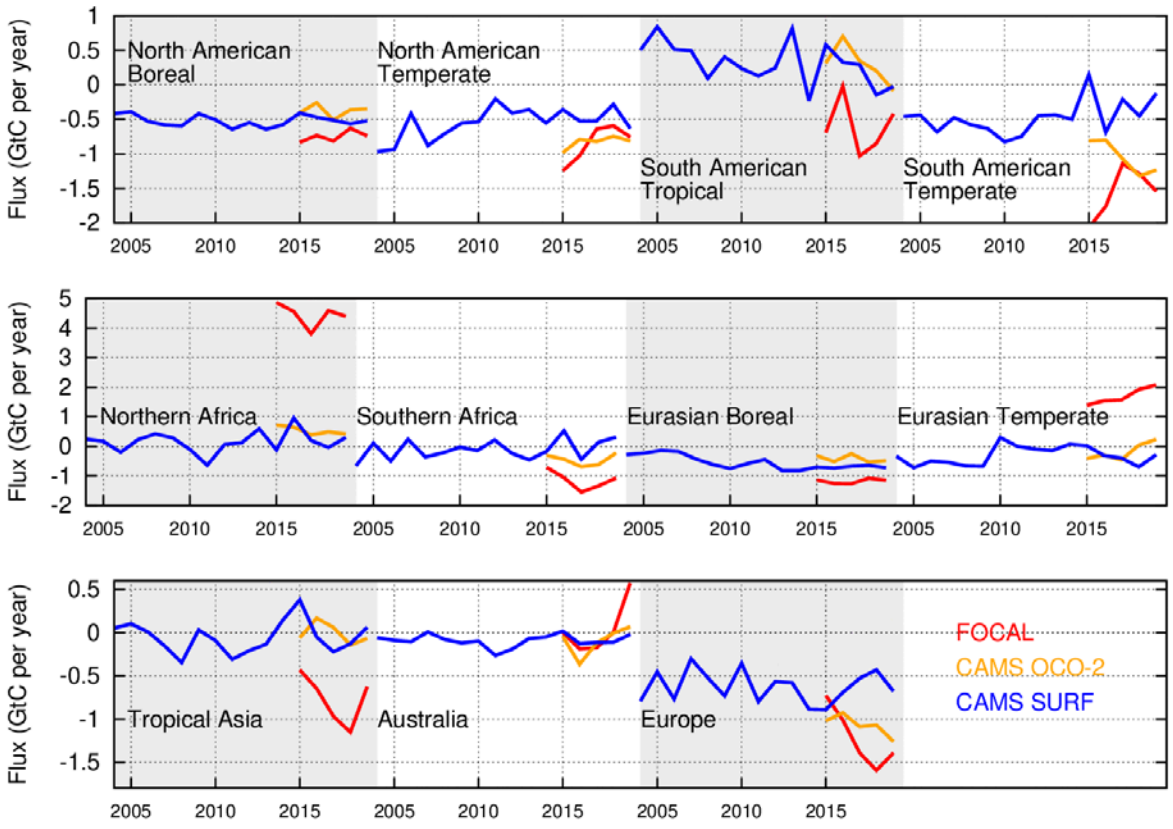

Figure 7. Inferred natural CO_2 annual flux (without fossil fuel emissions) averaged over the TransCom3 land regions. In the sign convention, positive fluxes correspond to a net carbon source into the atmosphere.

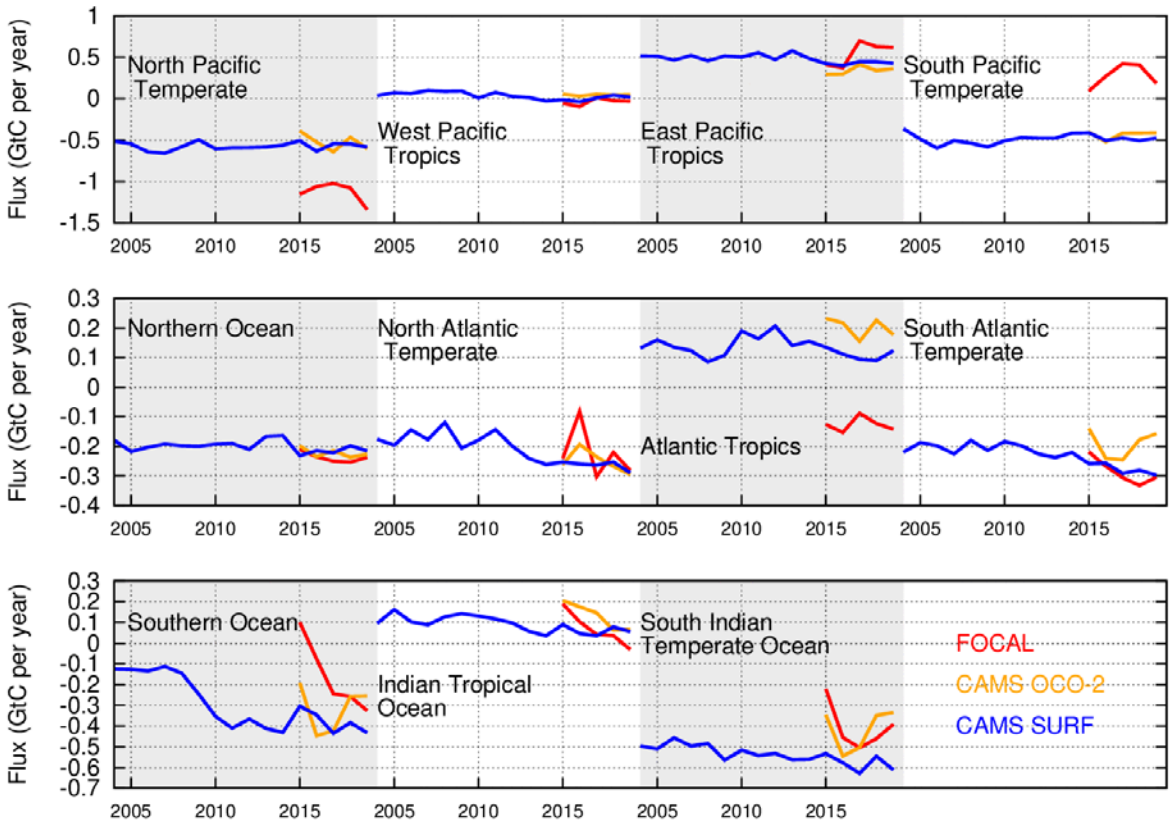

Figure 8. Same as Figure 7, but for the ocean basins.

3.3.5. Differences with aircraft measurements

Following the approach defined in Chevallier et al. (2019), we use continuous and flask dry-air-mole fraction measurements made by aircraft in the free troposphere to evaluate the three inversions over the 60-month period between January 2015 and December 2019. The free troposphere is simply defined here as the atmospheric layer between 2 and 7 km above sea level (asl). The measurements are those from ObsPack Globalview+ v6.0 for the full study period (Cooperative Global Atmospheric Data Integration Project, 2020), without any filter for outliers. We note that no aircraft data is assimilated here.

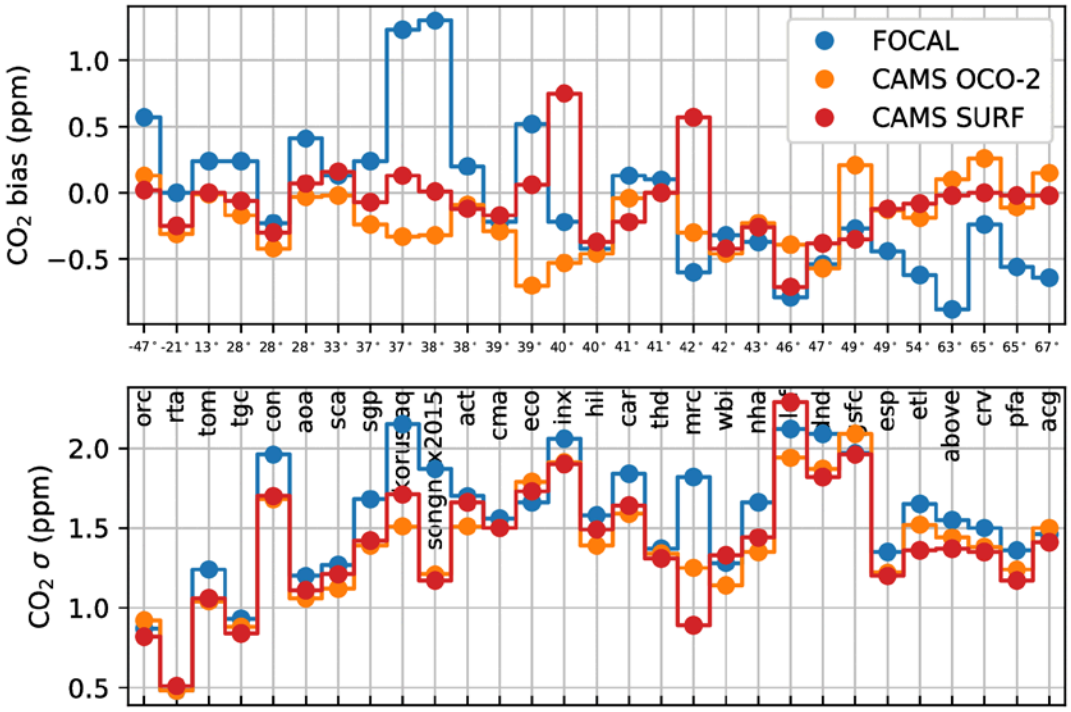

Figure 9. Mean and standard deviations of the model-minus-observation differences for the January 2015 – December 2019 period per measurement program for the CAMS ACOS-based inversion (orange line), the CAMS surface-based inversion (green line) and the CO2_OC2_FOCA-based inversion (blue line). The number of measurements per site, campaign or program varies between 7 (MRC) and 514,578 (CON). The programs are ranked by increasing mean latitude (North is on the right), irrespective of their latitudinal coverage (which is large of several tens of degrees for ORC, TOM and CON). These mean latitudes are shown in the middle of the panel.

The absolute biases (Figure 9, top) are all less than 1.4 ppm. They are usually even less than 0.8 ppm for the two CAMS inversions. There is no obvious latitudinal trend in the surface air-sample inversion, and therefore no obvious flaw of the model vertical mixing (Stephens et al., 2007). However, the ACOS inversion exhibits a fluctuating bias in the northern hemisphere (slightly negative below 39°N, slightly positive above 48°N and negative in-between) that suggests some errors in the distribution of the fluxes in this hemisphere. The bias of CO2_OC2_FOCA inversion seems to decrease with increasing latitudes above 37 °N that suggests a larger-scale error. Standard deviations vary with the fraction of land masses in a given latitude, as expected. They are about 1.5 ppm in the northern hemisphere for the three inversions, with the CO2_OC2_FOCA-driven numbers larger than the ACOS-driven numbers by ~ 0.2 ppm. When taking all free tropospheric aircraft data together, the posterior simulation deviates from the measurements by -0.1±1.4 ppm (mean bias ± √mean variance across

the aircraft programs, irrespective of their number of data), -0.2±1.4 ppm and -0.1±1.6 ppm for the ACOS-driven inversion, for the CO2_OC2_FOCA-driven inversion and for the surface-driven inversion, respectively.

3.3.6. Conclusions

The assimilation of the CO2_OC2_FOCA product in the LSCE global inversion system infers CO2 surface fluxes that are very different from those obtained by the assimilation of surface air-sample measurements. The CO2_OC2_FOCA-driven CO_2 surface fluxes appear to be less credible because (i) the inferred spatial distribution of the ocean outgassing regions is inconsistent with current knowledge of the marine biogeochemistry obtained from sea surface CO_2 partial pressure measurements (see the Global ocean surface carbon product of the Copernicus Marine Environment Monitoring Service[1], (ii) the inferred atmospheric growth rates for years 2017 and 2019 are notably different from the ones seen at marine background stations, (iii) the biases with aircraft data in the free troposphere are larger than when assimilating the surface measurements and show a dependency on latitude. In contrast, the ACOS-driven CO_2 surface fluxes (ACOS being restricted to land retrievals here) seem to perform better than the CO2_OC2_FOCA-driven fluxes and even show comparable difference statistics to aircraft measurements in the free troposphere in output to the transport model compared to surface-air-sample-driven fluxes. This result demonstrates that there is no fundamental limitation to atmospheric inverse modelling (e.g., in the realism of the transport model or in the modelled error statistics) when assimilating satellite XCO_2 retrievals. The ACOS-driven CO_2 surface fluxes have actually been part of the official CAMS data portfolio since year 2019.

The various tests performed do not allow us to identify the distinctive asset of ACOS vs. CO2_OC2_FOCA in our system: either the data density (much larger for ACOS over land), the data precision (that seem to be better for ACOS, see Section 3.2.2), the data trueness (linked both to the quality of the physical retrieval scheme and to its empirical bias-correction), the accuracy of the averaging kernels (see Chevallier, 2015, for a discussion on potential issues with the averaging kernel profiles), or a combination of these qualities at once. Detailed sensitivity tests could be performed for this, but note that our single CO2_OC2_FOCA-driven inversion already represented a large computational effort that lasted four weeks on a parallel cluster.

About computational effort, CO2_OC2_FOCA's distinct advantage compared to ACOS is its representation of multiple scattering effects in the radiative transfer in a form that is not costlier than absorption. In preparation for the Copernicus CO_2 Monitoring Mission that will provide even larger amount of data than OCO-2 (Pinty et al., 2017), CO2_OC2_FOCA represents an important achievement. In this context and resources permitting, it would be important to document its performance in more detail in order to help prioritize future developments.

[1] http://marine.copernicus.eu/services-portfolio/access-to-products/?option=com_csw&view=details&product_id=MULTIOBS_GLO_BIO_REP_015_005

4. Assessment of satellite-derived XCH_4 data products

4.1. Introduction

Global methane inversions based on satellite measurements are already long established, going back to the initial SCIAMACHY XCH_4 dataset from 2003, followed by over a decade of soundings from GOSAT, with improved stability and measurement precision, but sparser data coverage. With the launch of Sentinel-5 Precursor (S5P) in October 2017, these measurements moved from experimental measurements to an operational product, with vastly increased data density through a small footprint (7-km at nadir) and a continuous wide swath (2600 km). A year later, in October 2018, the Japanese satellite GOSAT-2 was launched, the successor to the successful GOSAT mission.

The 6th GHG-CCI+ Climate Research Data Package (CRDP#6, https://climate.esa.int/en/projects/ghgs/#data) includes the following three CH_4 products, resulting from these two sensors:

- CH4_S5P_WFMD: retrieved from TROPOMI on S5P using the University of Bremen's WFMD algorithm
- CH4_GO2_SRFP: retrieved from GOSAT-2 using SRON's full physics RemoTeC algorithm
- CH4_GO2_SRPR: from GOSAT-2 using SRON's proxy RemoTeC algorithm, retrieving the ratio of CH_4 to CO_2

Product ID	Instrument	Algorithm	Data provider	Reference	Period available	Evaluators (sections)
CH4_S5P_WFMD	TROPOMI	WFMD, v1.2	IUP, Univ. Bremen	Schneising et al., 2019	11/2017-07/2020	DLR (4.2, 4.3)
CH4_GO2_SRFP	GOSAT-2	V1.0	SRON	ATBD	02/2019-10/2019	DLR (4.2)
CH4_GO2_SRPR	GOSAT-2	V1.0	SRON	ATBD	02/2019-10/2019	DLR (4.2)
CH4_S5P_SRON	TROPOMI	RemoTeC 2.5.0	SRON	Hu et al., 2016	04/2018-into 2021	DLR (4.2, 4.3)
CH4_S5P_SRONt	TROPOMI	RemoTeC 14_14	SRON	Lorente et al., 2021	11/2017-10/2020	DLR (4.2, 4.3)

Table 2. XCH_4 products evaluated in this report. Only the first four belong to CRDP#6, but the two SRON retrievals of S5P measurements are included for context and completeness.

The GOSAT-2 retrievals are only available from February through October 2019 at this point, not long enough to perform global inversions. The CH4_S5P_WFMD data products is available over a longer time, from November 2017 through July 2020. To enrich the comparison, the operational retrieval of XCH_4 from S5P (Hu et al., 2016) is also included in the analysis, and will be referred to as CH4_S5P_SRON in the text, and as "SRON" in figures. Additionally, the "scientific" or pre-operational SRON retrieval, based on Lorente et al. (2020), is considered. This product includes some corrections for retrievals over high and low albedo scenes and updated spectroscopy, and extends the coverage

into the commissioning phase. It is referred to as CH4_S5P_SRONt (or simply SRONt) in this report. The evaluated XCH_4 products are summarized in Table 2.

4.2. Comparisons with forward model simulations

4.2.1. Method

In this section we begin by plotting the data products themselves, to get a view of the temporal and spatial distribution. We then compare the different satellite products with concentration fields resulting from a forward simulation of the TM3 transport model (Heimann and Körner, 2003) using optimized fluxes from an inversion assimilating flask measurements from 31 surface sites. The inversion was carried out using the Jena CarboScope variational inversion system (based on Rödenbeck et al., 2003). The transport is at 3.8° latitude by 5° longitude resolution and has 19 vertical levels, and is driven with meteorological fields from the ERA5 reanalysis.

Because the model transport is imperfect, especially with respect to the tropopause height and the gradient of methane within the stratosphere, the comparison to the surface-optimized fields is used to derive a model-specific bias correction. The bias correction is modelled as a 2nd order polynomial as a function of latitude and month, following the approach of Bergamaschi et al. (2007) (see Equation 4 in this paper). Because this correction is independent of longitude, the information about local gradients is largely maintained, while ensuring that the model can simultaneously interpret total-column and surface-based measurements of CH_4 consistently.

When comparing the modelled XCH_4 columns to the XCH_4 measurements, both the prior profile and the averaging kernel are taken into account. Because the spatial resolution of the S5P measurements is so much higher than that of the model fields, we average them to create super-observations for use in the inversion. This is done as follows:

- Count all retrievals with quality flag "good" (or, for CH4_S5P_SRON and CH4_S5P_SRONt, those with qa filter > 0.5) that fall within a model doxel (gridbox per orbit)
- Average the XCH_4 values, weighted by the inverse of measurement precision
- Calculate the mean averaging kernel, averaging per retrieval layer, weighted by the inverse of the measurement precision
- Determine the super-obs measurement precision, as the maximum of:
    - Double the weighted mean precision or
    - The standard deviation of the XCH_4 measurements in the doxel

4.2.2. Results

4.2.2.1. Overview of measurement coverage

The spatial and temporal coverage of the satellite retrievals considered in this section are depicted in Figure 10, from January 2018 through June 2020. The CH4_S5P_WFMD retrievals are actually available from November 2017 through July 2020, CH4_S5P_SRONt from November 2017 through October 2020, and CH4_S5P_SRON from April 2018 (as shown) into 2021. The analysis is restricted to this period due poor coverage and concerns about the quality of the satellite retrievals in the commissioning phase (see section 4.2.2.2 for details) and the lack of in-situ measurements to constrain the surface-based inversion in the more recent months (see Figure 11). At first glance the S5P retrievals appear quite similar, though there are more gaps in the measurements seen for CH4_S5P_SRON and CH4_S5P_SRONt. This is partially related to the stricter data screening over land in this retrieval, but is dominated by the fact that the CH4_S5P_WFMD product also performs retrievals over the ocean, greatly increasing the number of measurements. This also explains the larger data gap seen over the Southern Ocean in the CH4_S5P_SRON and CH4_S5P_SRONt products. Another difference in temporal coverage is found in early 2020: both the CH4_S5P_SRON and CH4_S5P_SRONt products have a gap in mid-January, 2020, with no retrievals passing the suggested quality filters from January 11th through January 18th. No such gap is found in the CH4_S5P_WFMD retrieval product, and the number of successful retrievals per day during this period is consistent with that earlier and later in the month.

Looking to the plots on the right-hand side, it is interesting to see that the variability within a latitude band has a somewhat different structure in the the S5P retrieval products. CH4_S5P_WFMD shows substantial variability between 30-50 degrees latitude throughout the year, with the most variability in the winter. This latitude band is characterized by substantial anthropogenic emissions, consistent with this signal.

One feature that emerges from both the mean XCH_4 plot and the standard deviation plot for CH4_S5P_SRON is a positive anomaly along the northernmost edge of the measurement range in late winter and spring. If true, this would be a tantalizing signal: high methane during a period when the ground is still largely frozen, and northern wetlands are assumed to be inactive (or at least less active). However, this is also a period characterized by snow and ice cover and the resultant low albedo in the near infrared. This signal is not seen in either the CH4_S5P_WFMD, and appears somewhat weaker in the CH4_S5P_SRONt plot, abruptly ceding to lower XCH_4 values for measurements made north of about 70 degrees latitude.

Perhaps most worrying is the appearance of sporadic very low concentrations starting after 2020 for the CH4_S5P_ SRONt product, associated with high values of standard deviation. Note that the data in Figure 10 have already been averaged to the TM3 doxels, as described in Section 4.2.1, suggesting that this increased scatter is not the result of only a few anomalous retrievals.

To assess this further, one month from this period is chosen for detailed analysis: May 2020. The number of good-quality (non-aggregated) retrievals per day, the daily global mean value and the standard deviation of all the retrievals per day for the three TROPOMI retrieval products are summarized as timeseries in Figure 11. While the global mean concentration for the CH4_S5P_WFMD retrieval is fairly stable over the month, the CH4_S5P_SRON and CH4_S5P_SRONt retrievals show quite some variability, with the global mean XCH_4 value dropping by more than 10 ppb from one day to the next, such as from May 7-8, or (for SRONt) from May 25-26. This difference could be the result of a difference in data coverage however: methane has a strong interhemispheric gradient, and e.g. if only retrievals from the southern hemisphere pass the quality filters for one day,

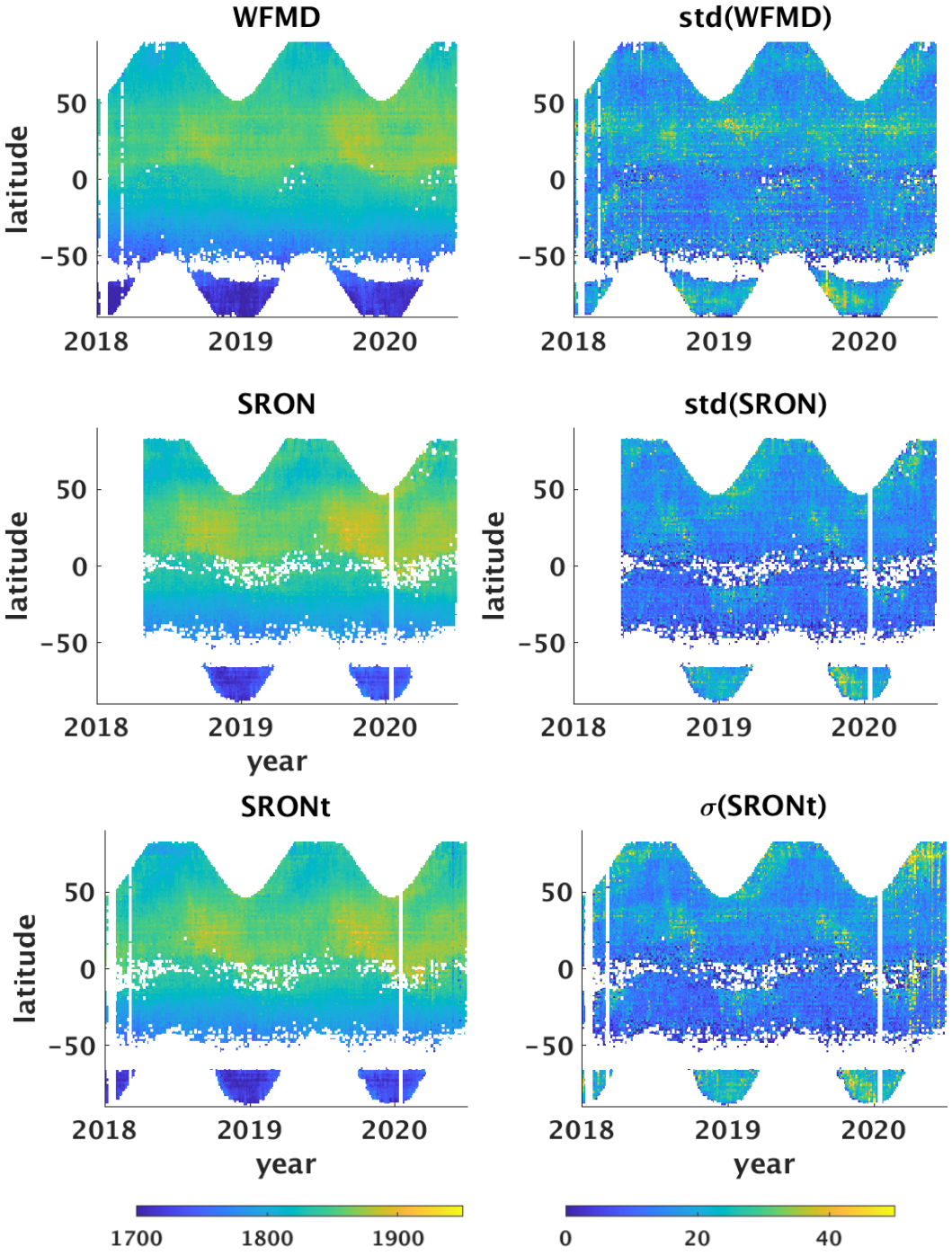

Figure 10: TROPOMI XCH_4 retrieval products considered here (from January 2018), averaged over 1 degree latitude and 3-day bins. The standard deviation of the measurements within each bin is shown on the right. Both quantities are in parts per billion (ppb), or 10^{-9} moles CH_4/mole of dry air. From the top are shown: CH4_S5P_WFMD, CH4_S5P_SRON, and CH4_S5P_SRONt.

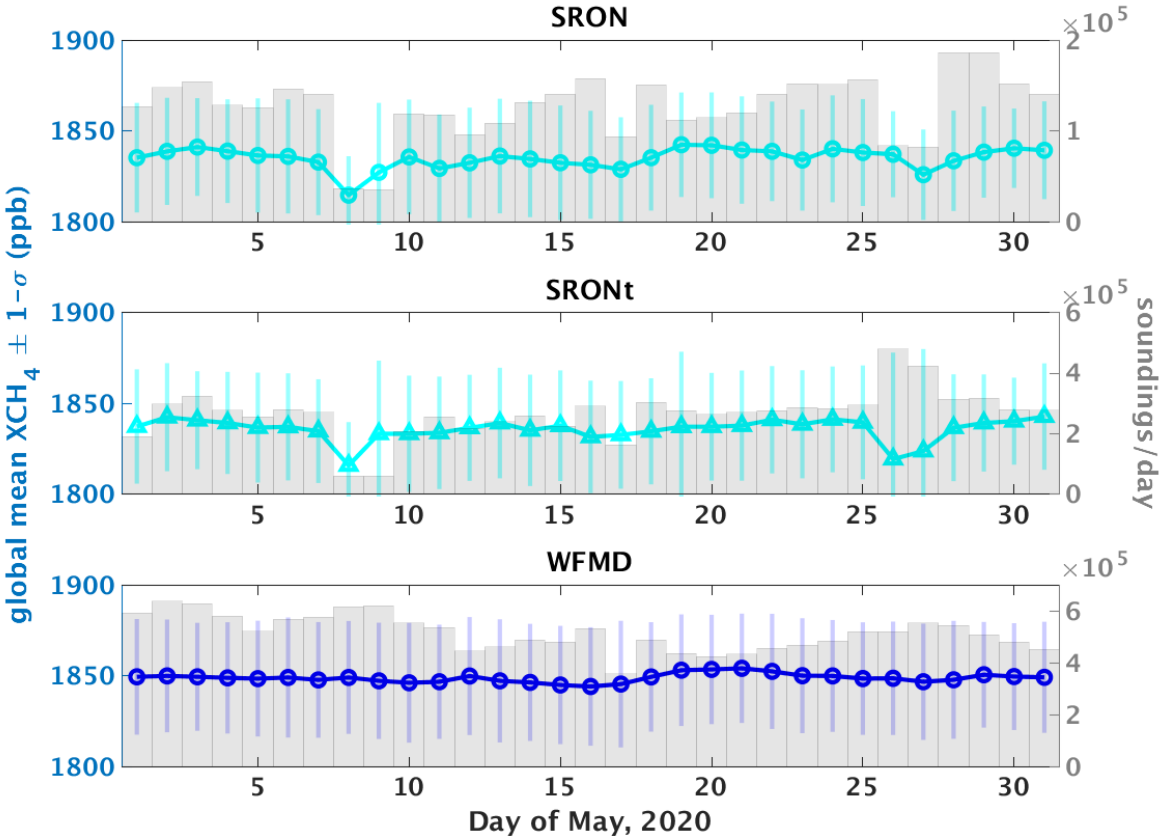

Figure 11: Global daily mean XCH_4 retrievals (on the left axis) for three different TROPOMI products in May, 2020, with the total number of retrievals per day shown as grey bars (on the right axis). The vertical bars on the daily means represent +/- one standard deviation.

this could result in a decrease. Indeed, the total number of soundings per day drops substantially from May 7-8 for the CH4_S5P_SRONt and CH4_S5P_SRON products. In contrast, the number of good retrievals increases from May 25-26 for SRONt (accompanied by a sharp drop in daily mean XCH_4) while decreasing for SRON (with the mean XCH_4 value remaining steady). May 26 also shows the highest single-day standard deviation for CH4_S5P_SRONt, with a value of 59 ppb. To see if data coverage can explain these differences, the soundings are binned onto 0.1°x0.1° bins and plotted in Figure 12. The colour range was chosen to highlight exceptionally low values, which can be seen for the CH4_S5P_SRONt retrieval in several areas, including the far western Amazon basin; around Montevideo, Uruguay; northern Poland; and northern Quebec (east of Hudson's Bay). The CH4_S5P_SRON and CH4_S5P_SRONt retrievals appear to agree well in regions where they both report good quality data, but the CH4_S5P_SRON is heavily screened, reporting good quality retrievals from neither the Americas nor Europe on this day. CH4_S5P_WFMD has more coverage than CH4_S5P_SRON, but does not report retrievals for the aforementioned regions. Nonetheless,

this difference in data coverage does not explain these extremely low values, which are found for some other days in 2020 as well.

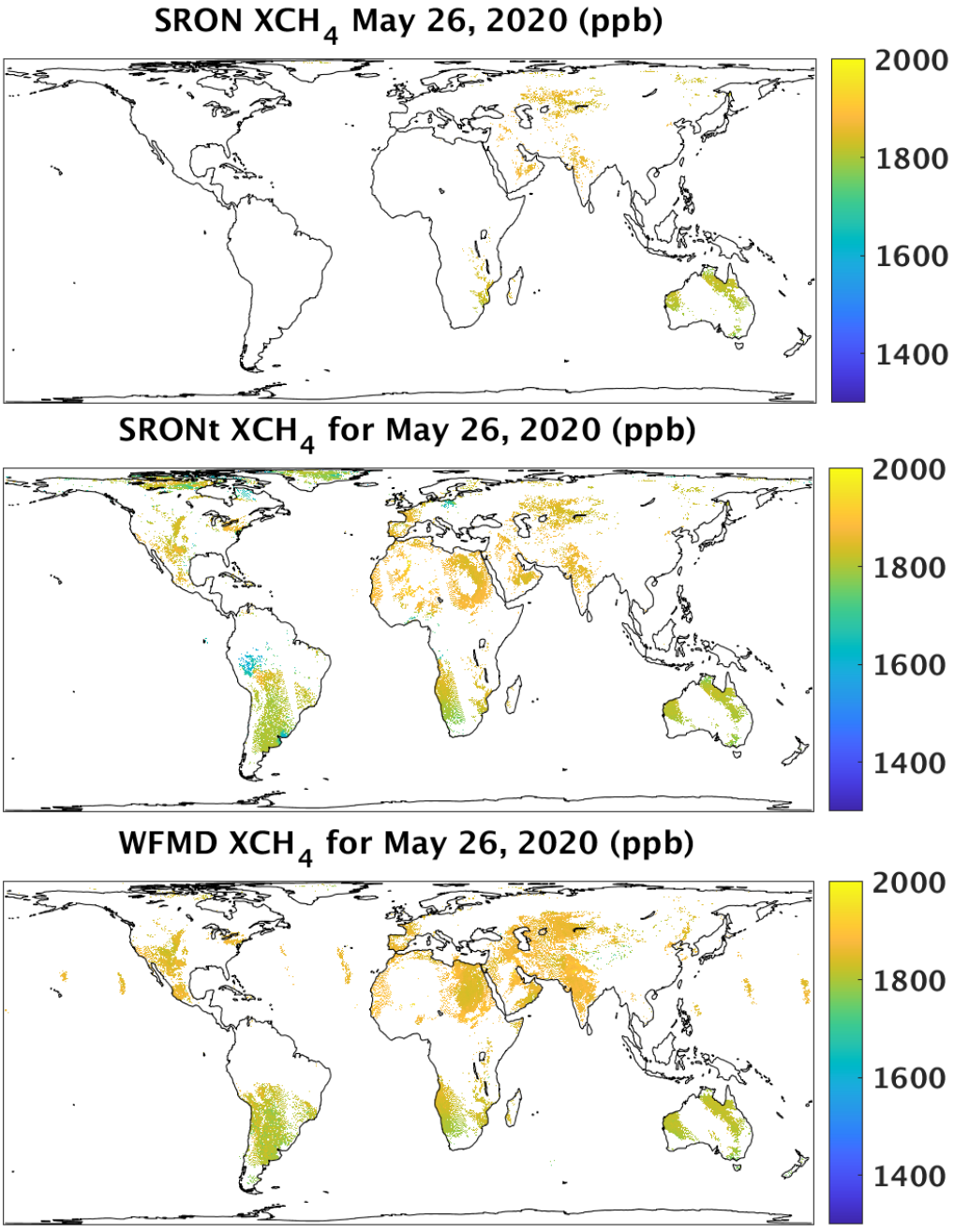

Figure 12: Daily mean XCH_4 on 0.1°x0.1° bins for the three TROPOMI retrievals on May 26, 2020.

To consider the results over the month as a whole, the zonal mean and zonal standard deviation at 0.1° resolution for the three products is shown in Figure 13. While all three products display a typical interhemispheric gradient with a noticeable decrease when passing the intertropical convergence zone (ITCZ) from north to south, CH4_S5P_SRONt clearly displays some anomalously low values in the Tropics and at very high latitudes, and the highest monthly zonal standard deviation. This

behaviour by CH4_S5P_SRONt is not seen throughout the entire record, but only from about April 2020, with some days being noticeably noisier than others. This can also be seen in Figure 10.

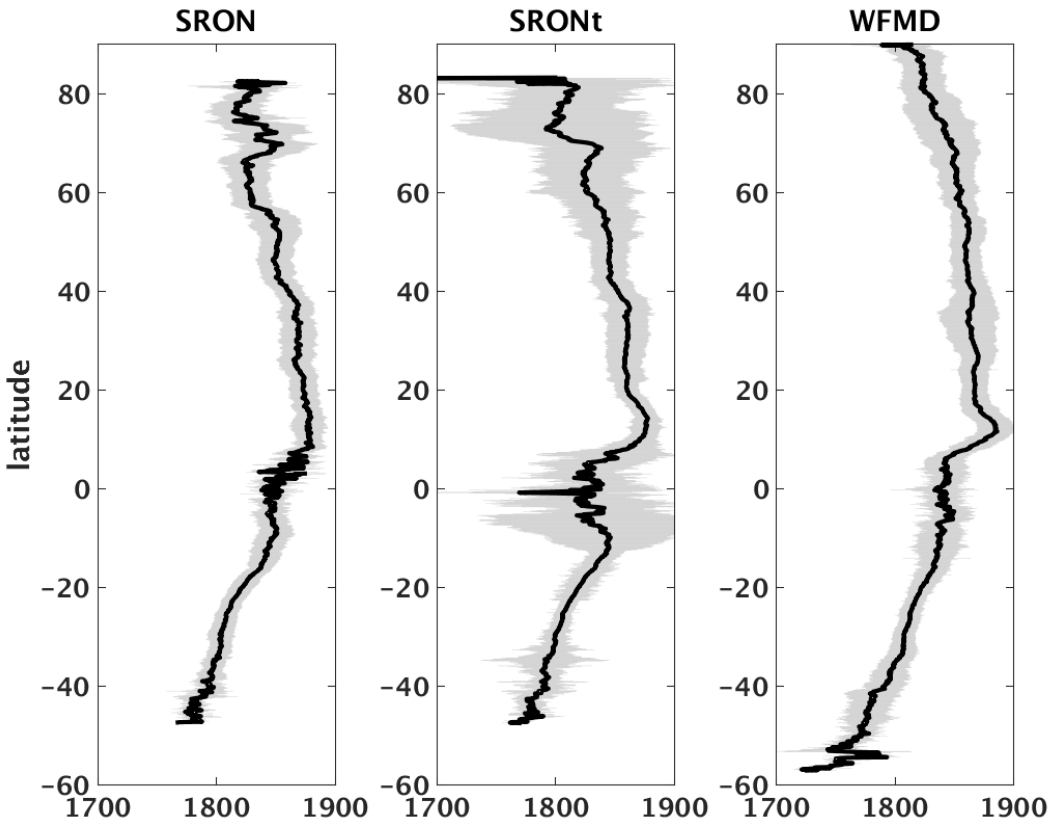

Figure 13: Zonal mean XCH_4 +/- one standard deviation in ppb for May 2020 for all three TROPOMI products.

For completeness, the coverage of the nine months of available GOSAT-2 data is shown in Figure 14. As expected, the proxy product (CH4_GO2_SRPR) has more measurements and thus, more coverage, than the full-physics retrieval (CH4_GO2_SRFP). Perhaps less expected, the proxy retrieval also exhibits the highest standard deviation within the averaging bins used here.

To explain why the inversions used here are limited to June 2020, while at least some of the satellite products are available beyond this point, the temporal and latitudinal coverage of the flask measurements used for the surface-based inversion and the ground-based FTIR measurements of the TCCON network are shown in Figure 15.

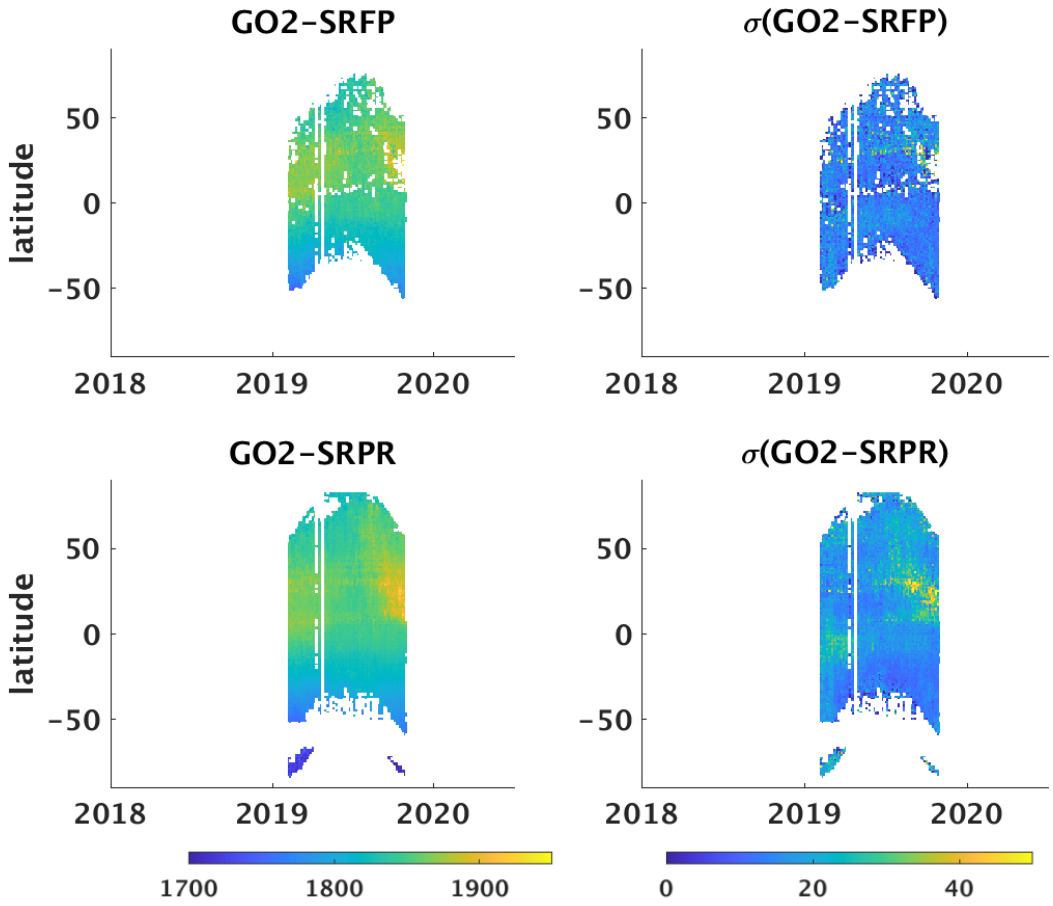

Figure 14: As Figure 10, but for the nine months of available GOSAT-2 retrievals for both the full physics retrieval (SRFP, top row) and the proxy retrieval (SRPR, lower panels).

4.2.2.2. Bias-correction based on surface-optimized fieldS

As described in Section 4.2.1, a 2nd-degree polynomial was fit to describe the mismatch between the XCH_4 retrievals and optimized model fields based on surface-only measurements. The analysis of this bias correction led to some insights about the data themselves.

In general, the bias correction is expected to have a similar shape for all the products, assuming they are roughly consistent with each other and have similar averaging kernels, as it is accounting for errors in the model's vertical structure and/or interhemispheric gradient. Likewise, the assumption that the error can be fit by month and latitude suggests that it ought to be similar for the same month in subsequent years. This is not what emerges when we look at the bias correction found for the CH4_S5P_WFMD retrieval, as seen in Figure 16. The curvature of the bias function for January through March 2018 is rather different to that found for the same period in 2019 and 2020. To ensure that this was not the effect of edge effects in the surface-based inversion at the start of the run, it was tested both with the prior and concentration fields from a longer inversion, and the result

was consistent. From April 2018 the curves are similar to those from the same months in other years, suggesting that it is the April 2018 data themselves that are inconsistent. On the positive side, the bias for the land and the ocean data are essentially identical throughout the rest of the data record, evidence for a lack of land-sea bias in the WFMD retrievals (not shown here).

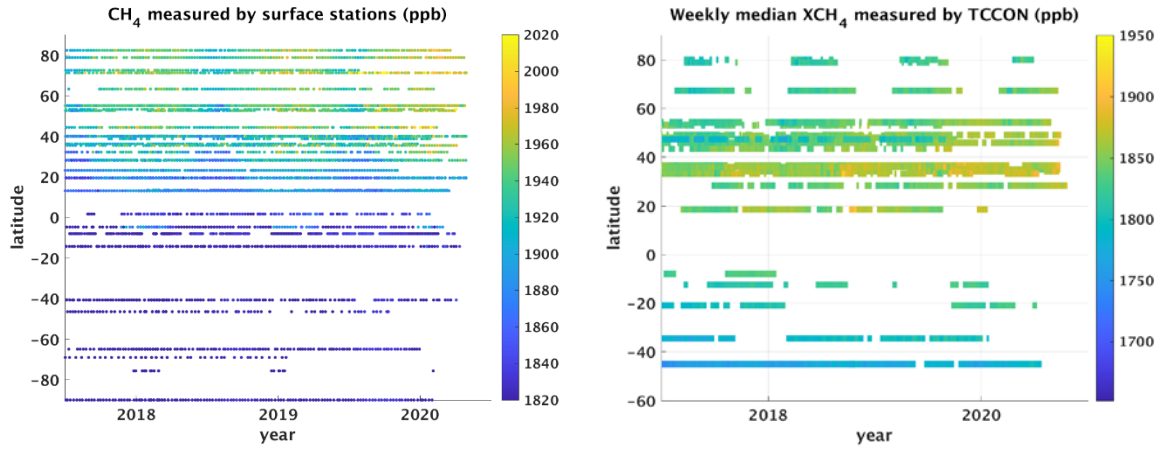

Figure 15: Spatial and temporal coverage of surface-based measurements used for the analysis, with 31 flask measurements used for the surface-based inversions on the left, and TCCON total column measurements on the right.

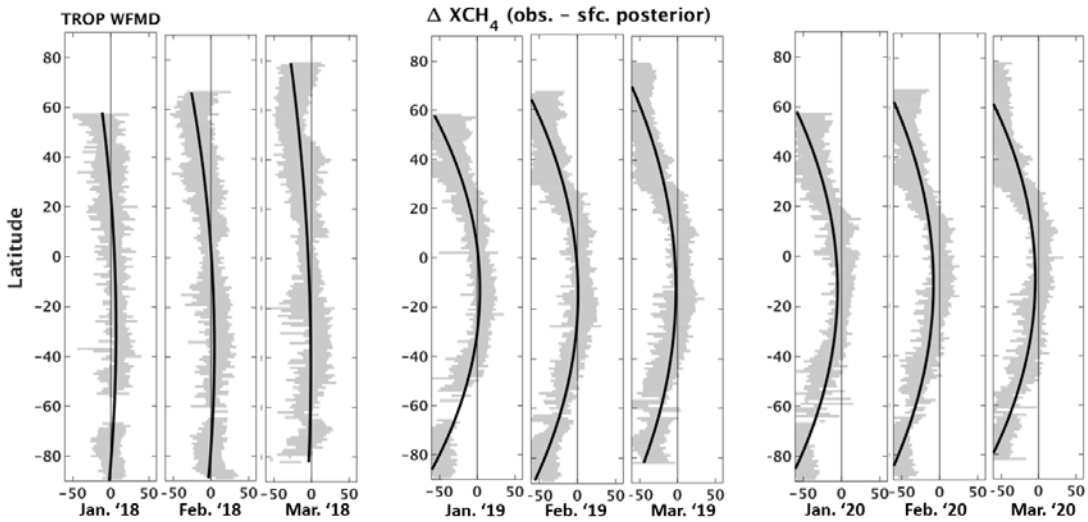

Figure 16: Bias correction for January-March for the years 2018, 2019 and 2020 for CH4_S5P_WFMD. The horizontal bars show one standard deviation of the spread in the data at 1-degree latitude bins. Note that the first three months of 2018 exhibit a different shape than the rest of the time series (not all shown), suggesting that the measurements during the pre-commissioning phase may not be consistent with the rest of the data record.

A similar analysis was carried out for the other products as well, and the behaviour of CH4_S5P_SRONt is similar for the beginning of 2018 (not shown).

The same curve-fitting was carried out for the offset between the GOSAT-2 retrievals and the surface-optimized concentration fields, as seen in Figure 17. In this case, the bias curve behaves as we would expect, similarly shaped throughout the months available. Encouragingly, the results for the SRPR and SRFP retrievals agree quite well. Large variability in both the SRFP and SRPR data is seen between approximately 20° and 30° latitude throughout the year, a signal that is not as appararent in the other data distributions.

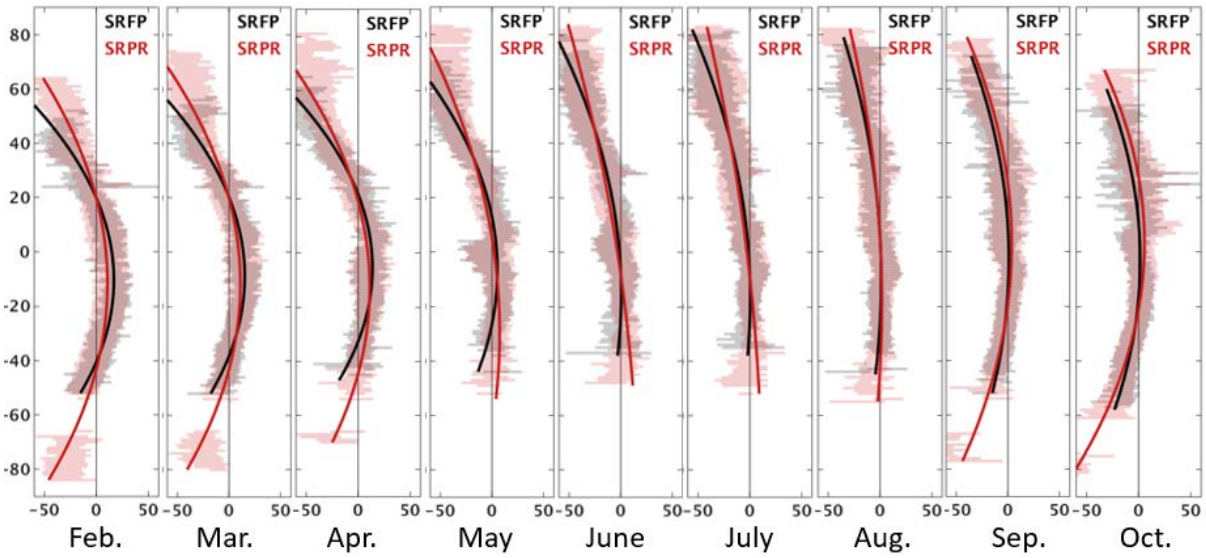

Figure 17: Bias-correction curves fit to the two GOSAT-2 retrieval products for 2019: CH4_GO2_SRFP and CH4_GO2_SRPR.

4.3. Methane inversion experiments with the Jena CarboScope

4.3.1. Method

After applying the bias corrections to the measurements, aggregated into super-observations, all three TROPOMI XCH_4 retrieval products were assimilated into the Jena CarboScope inversion system to attain optimized fluxes. The satellite data were assimilated alone, without combining them with other observations, in order to focus on the signals inherent to the measurements. From a scientific point of view this may not be the optimal approach: including continuous high-precision surface measurements can have a stabilizing effect on the results, but the goal of this assessment is to examine the retrieval products on their own merit.

The fluxes inferred from these satellite inversions are compared to the inversion over the same time period using the 31 flask sites, as described previously. This is quite a small station set for a surface-

based global inversion, but there are a limited number of surface sites with data already quality checked and available into mid-2020.

Following the CO_2 inversion analysis presented in Section 3.3, comparisons are made to: (i) data-driven estimates of mean global surface concentration and the resultant calculated growth rate, (ii) grid-point annual total fluxes, and (iii) the regional monthly CH_4 emissions.

4.3.2. Global mean atmospheric mixing ratio and growth rate

Similar to the approach for CO_2 in Section 3.3.2, the results from the inversions are compared to global estimates derived directly from the flask measurements. In this case, two estimates are used: NOAA estimates the monthly mean global concentration of methane near the surface based on measurements from its network of marine boundary layer sites (ref: *Ed Dlugokencky, NOAA/GML www.esrl.noaa.gov/gmd/ccgg/trends_ch4/)*. Similarly, the World Data Centre for Greenhouse Gas Measurements (WDCGG) provides a similar monthly measurement based on near-surface measurements, but includes more continental sites in their estimate, which leads to slightly higher estimates than NOAA's. The WDCGG estimates are reported in the annual WMO Greenhouse Gas Bulletin, and are regularly updated on the WDCGG website (https://gaw.kishou.go.jp/publications/global_mean_mole_fractions). Given the short time period available for the CRDP methane datasets being considered in the CAR, an analysis of monthly concentrations is attractive, even though we would expect this quantity to be less robust than an annual value.

To compare these to the optimized fields resulting from the inversion of the different products, the mean methane mixing ratio for each month is taken, averaged at the lowest model level over the whole globe, weighted by the area of the gridbox. The result of this comparison is shown in Figure 18. For reference, the concentrations resulting from the prior flux is included as well.

All the datasets show a similar seasonality, though the trend in the prior is negative. Most of the inversions show the typical double peak of the seasonal cycle, although it is only found in the NOAA estimate and not that of WDCGG. The offset between WDCGG and NOAA is as expected, as the former includes continental sites and not only marine background stations, and almost all methane emissions are on land. The agreement between the different inversions is good, although there are a few differences that stand out. The WFMD inversion is substantially higher than the others in December 2018, for example, but the biggest outlier is the May 2020 global mean concentration deduced from CH4_S5P_SRONt. This is certainly the result of the unrealistically low values seen in this product in April and May 2020, as discussed in detail in Section 4.2.2.2.

From these concentration values it is possible to estimate the annual growth rate by taking a running average of the first derivative of the monthly mean mixing ratios shown in Figure 18 over a 12-month period, centred around the month in question. Unlike CO_2, it is not possible simply to convert the net surface fluxes, as there is also an atmospheric chemical sink which imperfectly known and slightly non-linear. As such, the effective growth rate calculated from the global monthly mean surface

mixing ratios is more directly comparable to the growth rates estimated from NOAA and WDCGG. The result is shown in Figure 19.

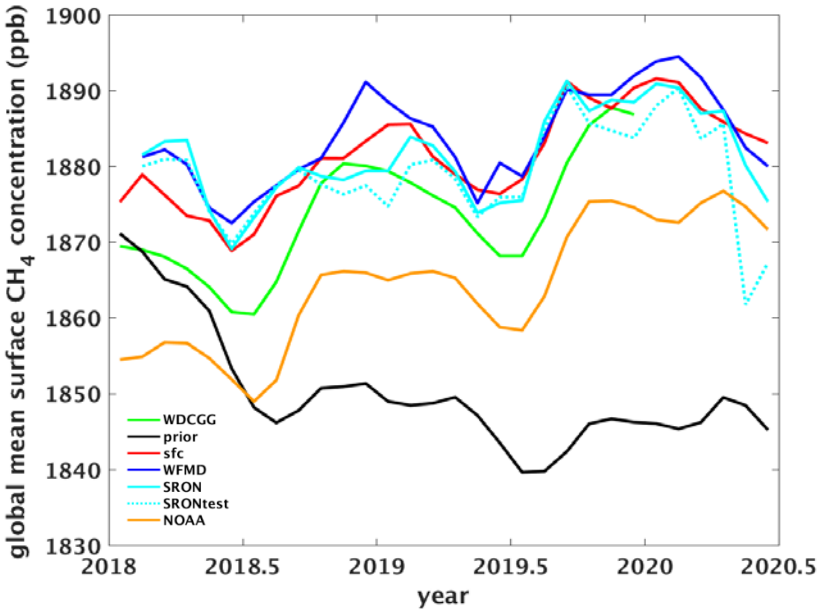

Figure 18: Monthly global mean surface CH_4 mixing ratio at the surface, based directly on in situ measurements (for NOAA in orange and WDGCC in green) or from forward simulations of the prior (in black) or optimized fluxes. The optimized fluxes are in turn constrained by different measurements, namely the surface network ("sfc", in red), CH4_S5P_WFMD ("WFMD", in blue), CH4_S5P_SRON ("SRON", the cyan solid line) or CH4_S5P_SRONt ("SRONtest", the cyan dashed line).

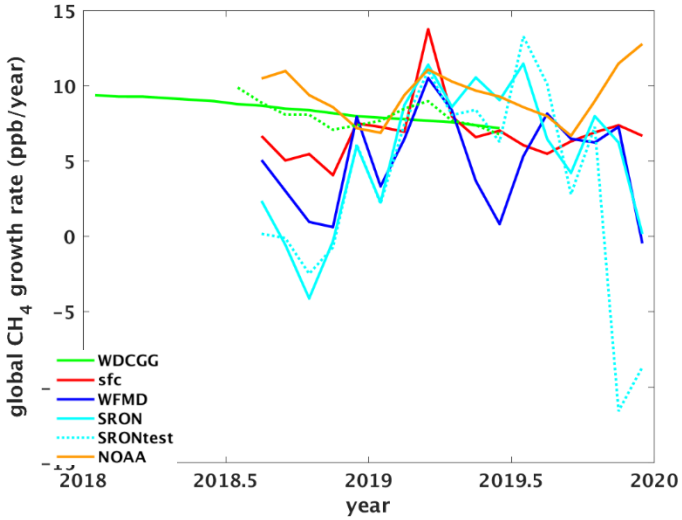

Figure 19: Annual growth rate of methane based on in situ measurements (for NOAA in orange and WDCGG in green), calculated as a 12-month running average of the derivative global mean surface mixing ratios from Figure 18. The solid green line is reported directly from the WDCGG whiel the dashed green line is calculated in the same manner as the other estimates.

Because six months before and after the month in question are needed to calculated the growth rate at a given point, the resultant time period is shorter. Nevertheless, there remains a 12- to 18-month period over which the growth rate estimates overlap, limited in recency by the WDCGG estimate. When averaged over the 12-month overlap period, the estimates all agree within a 1-σ uncertainty. There is even some agreement on higher time scales, like the high value for March 2019 which is seen across estimates. However, there is quite some variability from month to month, and towards the end of the record it looks as if the inversion results, especially those derived from TROPOMI, are diverging from the NOAA estimate. However, this includes the flux estimate from the last month of the inversion, which is poorly constrained by measurements and may show anomalous edge effects. Despite this caveat, the very low growth rate estimate based on the assimilation of CH4_S5P_SRONt does reflect the low measurement values towards the end of the inversion period.

4.3.3. Maps of annual budgets

To assess the spatial patterns inferred from the different inversions, the spatial pattern of the mean annual fluxes for 2019 are compared in Figure 20. As for the CO_2 inversions, the flux increments and the inferred gradients are much stronger for the satellite-based inversions than the surface-base inversion. This is partly the result of the increased data density: the surface-based inversion is constrained by only 31 sites, some of whose records did not even extend until the end of the inversion period. However, it can also be the the result of the model trying to fit unrealistic gradients in measurements.

What is encouraging: the different TROPOMI-based inversions and the surface-based inversion agree on the direction and location of some flux increments, such as the decrease of the prior emissions over China and an increase over the Middle East and Central Asia. Both of these are generally plausible results and have been suggested from other studies as well. Potentially less plausible is the inversion increasing fluxes in the Arctic Ocean (especially for the WFMD and SRON inversions), while simultaneously reducing emissions over much of Boreal North America and Eurasia. Given the strong seasonal variability in the satellite measurements at high latitudes, this may be an artefact, especially as no (year-round) surface-based measurements were assimilated in the satellite-based inversions, which can help stabilize unrealistic seasonal responses.

The TROPOMI-based inversions also agree on some of the increments in the Tropics: an increase in Tropical Asia and a general shift in the pattern of fluxes in the Amazon, leading to higher emissions close to the Atlantic Coast and lower emissions to the south and west. In Africa there is less consensus, though all simulations suggest large increments in the Congo Basin, a region of high uncertainty and large gradients, thanks to its proximity to the ITCZ.

Some other interesting signals that show up across TROPOMI inversions: an increase in emissions towards the western side of the Gulf of Mexico with a decrease to the east, suggesting that the measured gradients were not matched well by the prior.

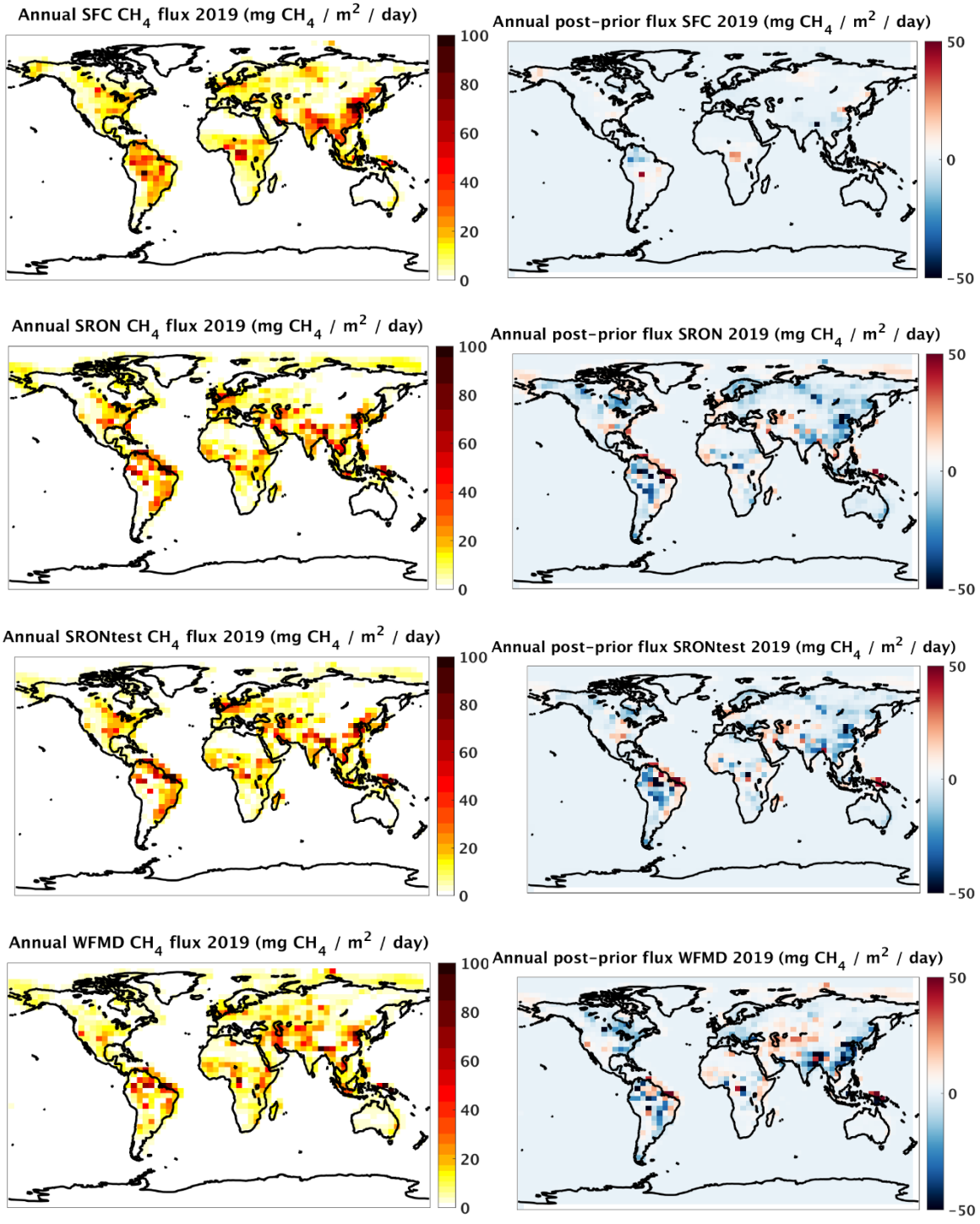

Figure 20, left side: annual flux maps for 2019 for the four inversions, from top to bottom: based on flask data, based on CH4_S5P_SRON, based on CH4_S5P_SRONt, based on CH4_S5P_WFMD. The right side shows the increment compared to the prior for the same simulations.

4.3.4. Monthly budget time series

As for CO_2, the CH_4 fluxes are aggregated onto the TransCom3 regions for comparison, however here the monthly fluxes are considered rather than the annual fluxes, partially because of the shorter timeseries. These are shown in Figure 21.

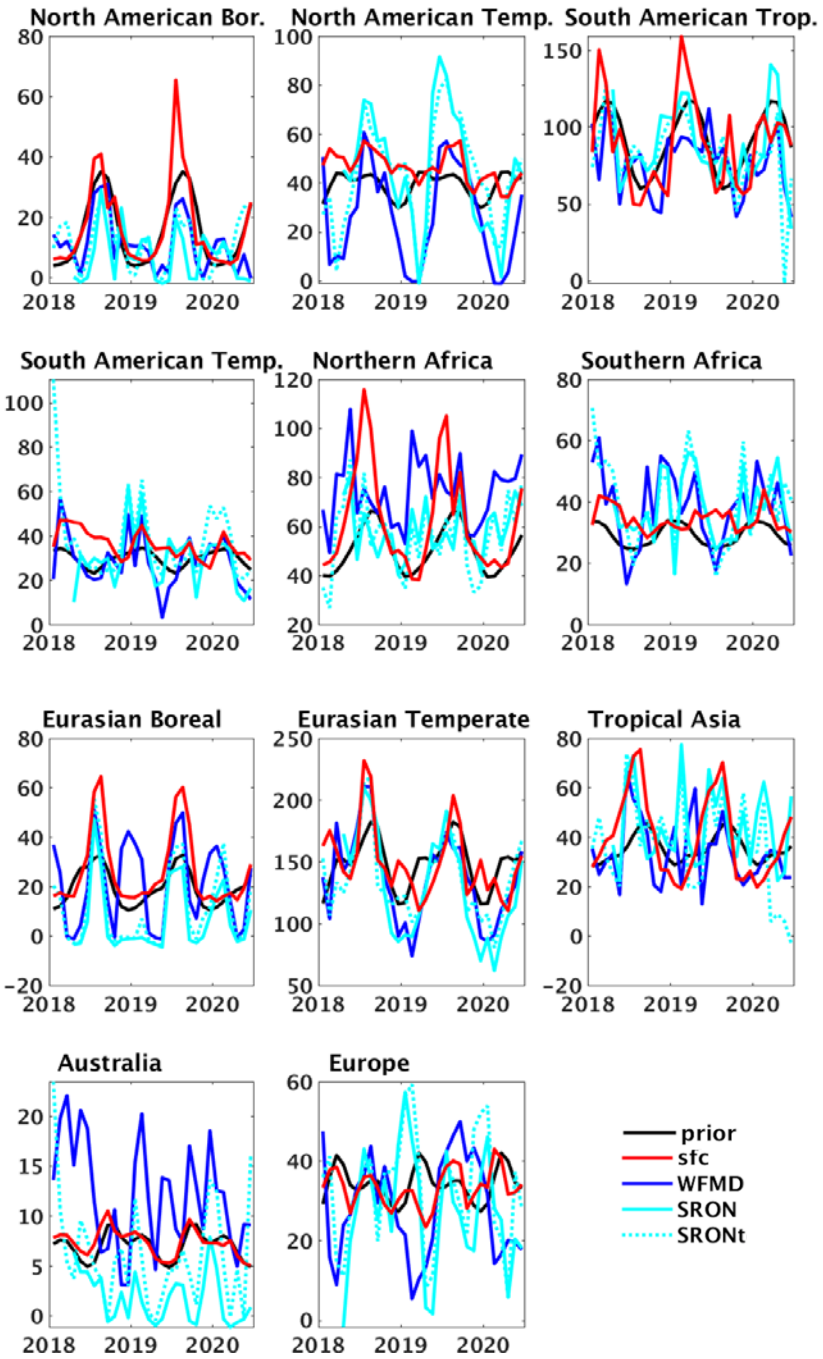

Figure 21: Monthly regional CH_4 fluxes (Tg CH_4/year) aggregated onto TransCom3 land regions (as shown in Figure 6).

Upon looking at the monthly fluxes on these scales, it is clear just how noisy the satellite-based retrievals are in time. (No in-situ data were assimilated simultaneously, which can have a stabilizing effect on the fluxes.)

Some adjacent regions appear to be anti-correlated with each other when compared to the prior (in black) or the surface-based inversion (in red). As an example, the satellite-based inversions suggest that the amplitude of the seasonal cycle in Boreal North America should be substantially reduced, but that the amplitude of the seasonal cycle in Temperate North America should approximately four times as strong as inferred from the surface-based measurements. This result is not likely to be true, especially given the fact that Temperate North America is one of the regions better constrained by surface measurements. Similarly, the satellite-derived European regional fluxes show an unrealistically large seasonal cycle.

The Eurasian Boreal region also shows an unexpected seasonal cycle with a large flux in the winter in the WFMD retrieval. This may be the result of a systematic bias at high latitudes, perhaps amplified by an imperfect latitude-dependent bias correction and seasonally-dependent data coverage. While there have been flux tower measurements of bursts of winter methane fluxes as wetland soils freeze, this signal is almost certainly not realistic, and is coming at a time when there are essentially no satellite measurements over the region. This anomalous seasonal cycle may be to blame for the high value in the global mean surface concentrations of methane seen for the CH4_S5P_WFMD-optimized fields in December 2018 in Figure 18.

The influence of the anomalously low values in the CH4_S5P_SRONt data in late spring and early summer 2020 can be seen in the extremely low fluxes in both Tropical South America and Tropical Asia towards the end of the timeseries.

4.3.5. Comparison with aircraft data and TCCON

Inspired by the approach undertaken for the CO_2 analysis in Section 3.3.5, both aircraft-based and total column TCCON measurements of XCH_4 are used to assess the performance of the different inversions. None of the measurements used here were assimilated in the inversion. Given the shorter time period of the methane inversions naturally there are less data sets available, but the approach is similar.

The comparison to the aircraft data, in Figure 22, shows that the surface-based inversion performs somewhat better than the satellite-based inversions, with on average lower bias and a smaller standard deviation, especially for mid-latitude sites. The worst performance for all inversions is for the aircraft measurements from Southern Great Plains, with a consistent low bias and very high standard deviation, likely due to the large amounts of oil and gas emissions in the region (Oklahoma, USA), leading to high variability which the coarse global model is unable to reproduce.

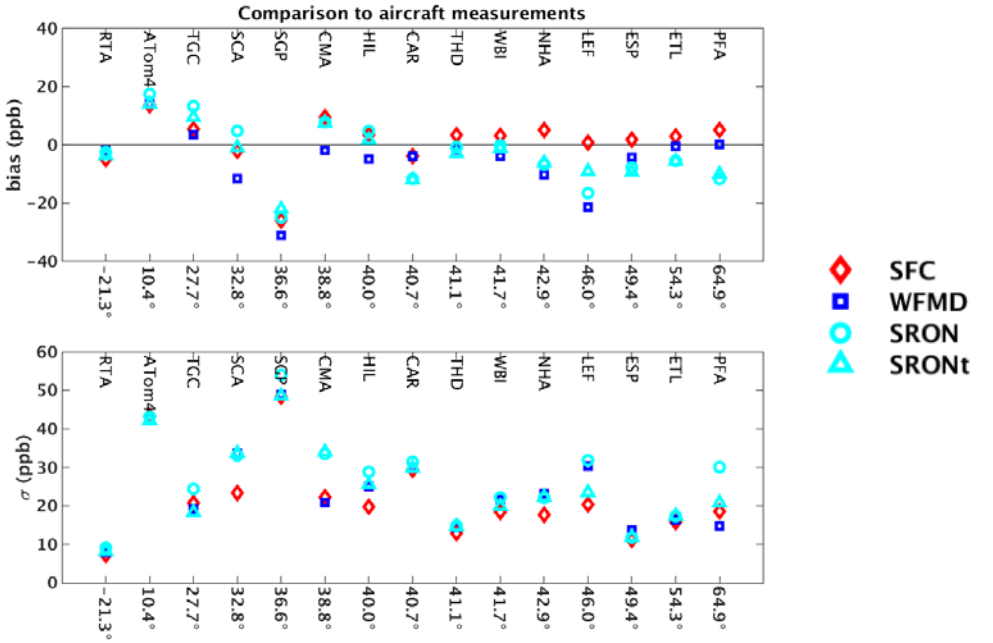

Figure 22: Comparison of optimized concentration fields to aircraft measurements, with mean bias (top panel) and standard deviation of the difference (bottom panel). The campaigns are sorted by latitude.

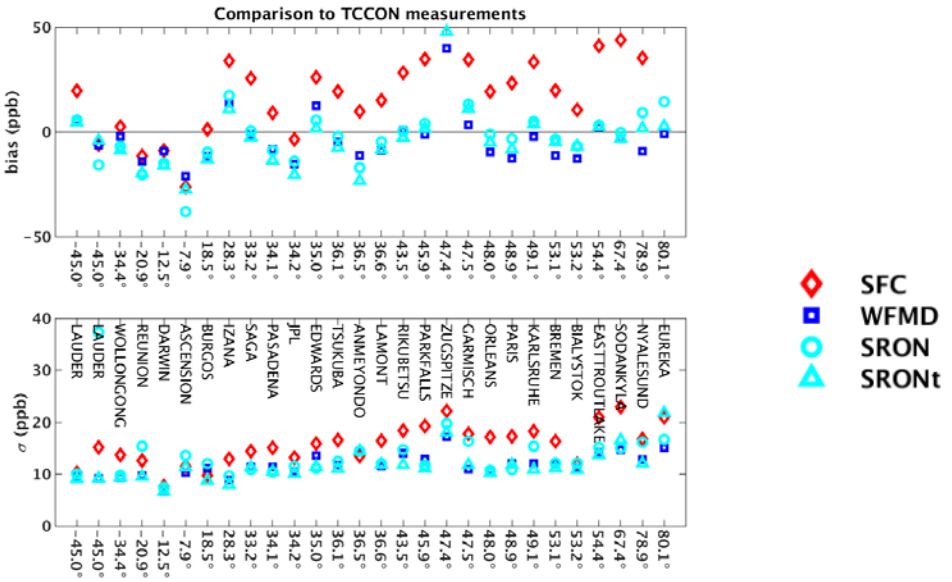

Figure 23: Comparison of optimized concentration fields from different inversions to TCCON total column measurements, with mean bias (top panel) and standard deviation of the difference (bottom panel). The stations are sorted by latitude. The station names are omitted from the upper panel for clarity. The station Lauder is listed twice, as the instrument was replaced during this period, and installed at a slightly different location. The two records overlap slightly in time.

High biases are also found for the ATom4 flight campaign, which are related to a poor representation of the position of the tropopause. The data were not filtered to include only mid-tropospheric values, as was done for the CO_2 comparison, and this flight campaign includes extremely high profiles. There is no clear evidence for an interhemispheric or latitude-dependent bias, but the measurements are also almost exclusively in the northern hemisphere.

The comparison to TCCON measurements is shown in Figure 23. Contrary to the aircraft data, the concentration fields from the satellite-based inversions clearly agree with the measurements better than those from the surface-based inversion. Both the bias and the standard deviation are consistently smaller. This is not unexpected: a bias-correction was added to the satellite products to make them consistent with the surface-based inversion, which already indicates a model-specific inconsistency between the surface concentrations and the total column concentrations. And while TCCON data are not used directly to bias-correct the current generation of satellite retrievals, they are still employed as a quality check to ensure general consistency. As such a solution to the inversion problem that minimizes the model-data mismatch to the satellite columns is also expected to agree well with the independent total column measurements of TCCON.

At the same time, the good agreement suggests that there is no significant drift of the measurements over time, for example. The one station with very poor agreement is a mountain site (Zugspitze), at which representation errors of the total column are expected.

In the comparisons with the independent aircraft-based and TCCON data, no clear "winner" amongst the satellite products can be determined. While problems with the data record for CH4_S5P_SRONt towards the end of the inversion period are apparent, most of the available TCCON time series ended before the worst of this, as can be seen in the temporal coverage of the TCCON data, which is shown in Figure 15.

4.3.6. Conclusions

The fluxes produced by assimilating the various TROPOMI XCH_4 products into the Jena CarboScope show some general structural agreement with each other, but diverge significantly from the fluxes based on the assimilation of surface-based measurements. While the satellite-based fluxes are better able to match the (mostly) independent TCCON total column measurements, the surface-based inversion does slightly better in reproducing independent aircraft measurements. This analysis of the resultant fields with independent data does not show that any one retrieval product clearly outperforms the others, at least on the metrics considered here. The broader spatial coverage of the CH4_S5P_WFMD retrieval, including (consistent) retrievals over the oceans, makes it an attractive product for analysis.

Despite these positive findings in concentration space, the temporal and spatial variability of the fluxes that arise from the assimilation of TROPOMI XCH_4 are not consistent with our understanding of the methane budget and the expected variability of the fluxes driving it. The resultant variability is extremely high in both space and time, leading to unrealistically large seasonal cycles for several

regions. These differences are in some ways exaggerated by the experimental setup: the XCH_4 products were assimilated alone, without including the stabilizing influence of simultaneously assimilated surface measurements. Because the spatial coverage of the measurements has such a strong seasonal cycle, small systematic errors, especially at high latitude, or in regions with high prior uncertainties, like the Tropics, may lead to significantly biased results.

Based on the analysis perfomed here, there is some concern about the consistency of the measurements prior to April 2018 with the latter record: the curvature of the deduced model-specific latitude-dependent bias correction appears to be significantly different for both the CH4_S5P_SRON and CH4_S5P_WFMD retrievals, when compared to the same correction from following years. This needs to be further investigated to be sure that it is not an edge effect related to the spinup of the inversion, which cannot yet be fully discounted.

There also seems to be some problem with low biases for some days and regions in the CH4_S5P_SRONt product from April through June 2020. This assessment did not assess the records from more recent months, but it would be advisable to check if this is an ongoing problem, and if something has changed in the data screening compared to earlier retrievals, that do not show this behaviour. The low values are clearly not physically reasonable, and affect the deduced fluxes quite significantly. Here a case study was presented looking at one particular day, but there are a handful of such negative anomalies throughout the last three months of the data record of this retrieval.

Despite these concerns, the amount of detailed information about local methane gradients in these products is extraordinary, and the products have already found application for the analysis of point sources and local-scale gradients. They are also able to well reproduce global mean mixing ratios over the two and a half years considered in this report. However, for their application in global inversion modelling to analyse regional scale fluxes over seasonal and interannual scales, care needs to be taken to ensure that (perhaps small) systematic errors do not bias the resultant fluxes.

Acknowledgements

F. Chevallier thanks M. Reuter and M. Buchwitz for constructive discussions about the use and the evaluation of these products. He is very grateful to the many people involved in the air-sample measurements and in the archiving of these data. Some of the computations of Sections 3.2 and 3.3 have been performed using HPC resources from CCRT under the allocation A0090102201 made by GENCI (Grand Equipement National de Calcul Intensif). The OCO-2 ACOS data have been obtained from http://co2.jpl.nasa.gov. They were produced by the OCO-2 project at the Jet Propulsion Laboratory, California Institute of Technology. CAMS data are publicly available from http://atmosphere.copernicus.eu/.

References

Alexe, M., P. Bergamaschi, A. Segers, et al., Inverse modeling of CH_4 emissions for 2010–2011 using different satellite retrieval products from GOSAT and SCIAMACHY, *Atmos. Chem. Phys.*, 15, 113–133, doi:10.5194/acp-15-113-2015, 2015.

Bastos, A., Running, S.W., Gouveia, C. and Trigo, R.M: The global NPP dependence on ENSO: La-Nina and the extraordinary year of 2011. *J. Geophys. Res*. 118, 1247–1255, 2013

Basu, S., Guerlet, S., Butz, A., et al., Global CO_2 fluxes estimated from GOSAT retrievals of total column CO_2, *Atmos. Chem. Phys.*, 13, 8695-8717, 2013.

Basu, S., Krol, M., Butz, A., et al., The seasonal variation of the CO_2 flux over Tropical Asia estimated from GOSAT, CONTRAIL and IASI, *Geophys. Res. Lett.*, doi: 10.1002/2013GL059105, 2014.

Bergamaschi, P., C. Frankenberg, J. F. Meirink, M. Krol, M. G. Villani, S. Houweling, F. Dentener, E. J. Dlugokencky, J. B. Miller, L. V. Gatti, A. Engel, and I. Levin: Inverse modeling of global and regional CH_4 emissions using SCIAMACHY satellite retrievals, *J. Geophys. Res*., 114, doi:10.1029/2009JD012287, 2009.

Bergamaschi, P., et al.: Inverse modeling of European CH_4 emissions 2001-2006, *J. Geophys. Res*., 115(D22309), doi:10.1029/2010JD014180, 2010.

Bergamaschi, P., S. Houweling, A. Segers, M. Krol, C. Frankenberg, R. A. Scheepmaker, E. Dlugokencky, S. Wofsy, E. Kort, C. Sweeney, T. Schuck, C. Brenninkmeijer, H. Chen, V. Beck and C. Gerbig, Atmospheric CH_4 in the first decade of the 21st century: Inverse modeling analysis using SCIAMACHY satellite retrievals and NOAA surface measurements, *J. Geophys. Res*., 118, doi:10.1002/jgrd.50480, 2013.

Bloom, A. A., Palmer, P. I., Fraser, A., and Reay, D. S.: Seasonal variability of tropical wetland CH4 emissions: the role of the methanogen-available carbon pool, *Biogeosciences*, 9, 2821–2830, doi:10.5194/bg-9-2821-2012, 2012

Boden, T. A., Marland, G., and Andres, R. J.: Global, regional, and national fossil-fuel CO2 emissions. Carbon Dioxide Information Analysis Center, Oak Ridge National Laboratory, U.S. Department of Energy, Oak Ridge, Tenn., U.S.A., Doi:10.3334/CDIAC/00001_V2013, 2013

Buchwitz, M., M. Reuter, O. Schneising, et al., The Greenhouse Gas Climate Change Initiative (GHG-CCI): comparison and quality assessment of near-surface-sensitive satellite-derived CO_2 and CH_4 global data sets, *Remote Sensing of Environment*, 162, 344–362, doi:10.1016/j.rse.2013.04.024, 2015.

Buchwitz, M., M. Reuter, O. Schneising, W. Hewson, R.G. Detmers, H. Boesch, O.P. Hasekamp, I. Aben, H. Bovensmann, J.P. Burrows, A. Butz, F. Chevallier, B. Dils, C. Frankenberg, J. Heymann, G. Lichtenberg,

M. De Mazière, J. Notholt, R. Parker, T. Warneke, C. Zehner, D.W.T. Griffith, N.M. Deutscher, A. Kuze, H. Suto, D. Wunch, 2017: Global satellite observations of column-averaged carbon dioxide and methane: The GHG-CCI XCO_2 and XCH_4 CRDP3 data set, Remote Sensing of Environment, 203, 276-295, doi:dx.doi.org/10.1016/j.rse.2016.12.027.

Buchwitz, M., Dils, B., Reuter, M., Schneising, O., Preval, S., Boesch, H., Krisna, T.C., Aben, I., Product Validation and Intercomparison Report (PVIR) for the Essential Climate Variable (ECV) Greenhouse Gases (GHG): XCO_2 and/or XCH_4 from OCO-2, TanSat, Sentinel-5-Precursor and GOSAT-2, v2.0, 2 February 2021, 2021.

Butz, A., Guerlet, S., Hasekamp, O., et al., Toward accurate CO_2 and CH_4 observations from GOSAT, *Geophys. Res. Lett.*, doi:10.1029/2011GL047888, 2011.

Canadell, J. G., Ciais, P., Dhakal, S., et al., Interactions of the carbon cycle, human activity, and the climate system: a research portfolio, *Curr. Opin. Environ. Sustainabil.*, 2, 301–311, 2010.

Chevallier, F., et al.: Inferring CO_2 sources and sinks from satellite observations: method and application to TOVS data. *J. Geophys. Res.*, 110, D24309, 2005.

Chevallier, F.: Impact of correlated observation errors on inverted CO2 surface fluxes from OCO measurements, *Geophys. Res. Lett.*, 34, L24804, doi:10.1029/2007GL030463, 2007.

Chevallier, F., Maksyutov, S., Bousquet, P., Bréon, F.-M., Saito, R., Yoshida, Y., and Yokota, T.: On the accuracy of the CO_2 surface fluxes to be estimated from the GOSAT observations. *Geophys. Res. Lett.*, 36, L19807, doi:10.1029/2009GL040108, 2009.

Chevallier, F., et al.: CO_2 surface fluxes at grid point scale estimated from a global 21-year reanalysis of atmospheric measurements. *J. Geophys. Res.*, 115, D21307, doi:10.1029/2010JD013887, 2010a.

Chevallier, F., Feng, L., Boesch, H., Palmer, P., and Rayner, P.: On the impact of transport model errors for the estimation of CO_2 surface fluxes from GOSAT observations. *Geophys. Res. Lett.*, 37, L21803, doi:10.1029/2010GL044652, 2010b.

Chevallier, F., Deutscher, N. M., Conway, T. J., Ciais, P., Ciattaglia, L., Dohe, S., Frohlich, M., Gomez-Pelaez, A. J., Griffith, D., Hase, F., Haszpra, L., Krummel, P., Kyro, E., Labuschagne, C., Langenfelds, R., Machida, T., Maignan, F., Matsueda, H., Morino, I., Notholt, J., Ramonet, M., Sawa, Y., Schmidt, M., Sherlock, V., Steele, P., Strong, K., Sussmann, R., Wennberg, P., Wofsy, S., Worthy, D., Wunch, D., and Zimnoch, M.: Global CO_2 fluxes inferred from surface air-sample measurements and from TCCON retrievals of the CO_2 total column, *Geophys. Res. Lett.*, 38, L24810, doi:10.1029/2011GL049899, 2011

Chevallier, F., and O'Dell, C. W., Error statistics of Bayesian CO_2 flux inversion schemes as seen from GOSAT, *Geophys. Res. Lett.*, doi: 10.1002/grl.50228, 2013.

Chevallier, F., Palmer, P.I., Feng, L., Boesch, H., O'Dell, C.W., Bousquet, P., Towards robust and consistent regional CO_2 flux estimates from in situ and space-borne measurements of atmospheric CO_2, *Geophys. Res. Lett.*, 41, 1065-1070, DOI: 10.1002/2013GL058772, 2014a.

Chevallier, F., Buchwitz, M., Bergamaschi, et al., User Requirements Document for the GHG-CCI project of ESA's Climate Change Initiative, version 2 (URDv2), 28. August 2014, 2014b.

Chevallier, F.: On the statistical optimality of CO_2 atmospheric inversions assimilating CO_2 column retrievals, Atmos. Chem. Phys., 15, 11133–11145, https://doi.org/10.5194/acp-15-11133-2015, 2015.

Chevallier, F., Bergamaschi, P., Kaminiski, T., Scholze, M., Climate Assessment Report (CAR) for the GHG-CCI project of ESA's Climate Change Initiative, version 1.1 (CARv1.1), 18. Nov. 2013, 2013.

Chevallier, F., P. Bergamaschi, D. Brunner, S. Gonzi, S. Houweling, T. Kaminski, G. Kuhlmann, T. T. van Leeuwen, J. Marshall, P. I. Palmer, and M. Scholze, Climate Assessment Report for the GHG-CCI project of ESA's Climate Change Initiative, pp. 87, version 2, 22 April 2015, 2015.

Chevallier, F., M. Alexe, P. Bergamaschi, D. Brunner, L. Feng, S. Houweling, T. Kaminski, W. Knorr, T. T. van Leeuwen, J. Marshall, P. I. Palmer, M. Scholze, A.-M. Sundström and M. Voßbeck, Climate Assessment Report for the GHG-CCI project of ESA's Climate Change Initiative, pp. 94, version 3, 3 May 2016, 2016.

Chevallier, F., P. Bergamaschi, D. Brunner, L. Feng, S. Houweling, T. Kaminski, W. Knorr, J. Marshall, P. I. Palmer, S. Pandey, M. Reuter, M. Scholze, and M. Voßbeck, Climate Assessment Report for the GHG-CCI project of ESA's Climate Change Initiative, pp. 96, version 4,, 27 March 2017, 2017.

Chevallier, F., Climate Assessment Report for the GHG-CCI+ project of ESA's Climate Change Initiative, pp. 36, version 1.2, 20 March 2020, 2020.

Chevallier, F., Validation report for the inverted CO_2 fluxes, v20r1. CAMS deliverable CAMS73_2018SC2_ D73.1.4.1-2019-v4_202011. http://atmosphere.copernicus.eu/, 2020.

Chevallier, F., Remaud, M., O'Dell, C. W., Baker, D., Peylin, P., and Cozic, A.: Objective evaluation of surface- and satellite-driven carbon dioxide atmospheric inversions, Atmos. Chem. Phys., 19, 14233–14251, https://doi.org/10.5194/acp-19-14233-2019, 2019.

Cogan, A. J., Boesch, H., Parker, R. J., et al., Atmospheric carbon dioxide retrieved from the Greenhouse gases Observing SATellite (GOSAT): Comparison with ground-based TCCON observations and GEOS-Chem model calculations, *J. Geophys. Res.*, 117, D21301, doi:10.1029/2012JD018087, 2012.

Conway, T. J., Tans, P. P., Waterman, L. S., Thoning, K. W., Kitzis, D. R., Masarie, K. A. and Zhang, N.: Evidence for interannual variability of the carbon cycle from the National Oceanic and Atmospheric Administration/Climate Monitoring and Diagnostics Laboratory Global Air Sampling Network, *J. Geophys. Res*., 99(D11), 22,831–22,855, doi:10.1029/94JD01951, 1994

Cramer, W., Kicklighter, D. W., Bondeau, A., Iii, B. M., Churkina, G., Nemry, B., Ruimy, A., Schloss, A. L. and Intercomparison, ThE. P. OF. ThE. P. NpP. M., Comparing global models of terrestrial net primary productivity (NPP): overview and key results. *Global Change Biology*, 5: 1–15. doi:10.1046/j.1365-2486.1999.00009.x, 1999.

Cressot, C., F. Chevallier, P. Bousquet, et al., On the consistency between global and regional methane emissions inferred from SCIAMACHY, TANSO-FTS, IASI and surface measurements, *Atmos. Chem. Phys.*, 14, 577-592, 2014.

Cressot, C., Pison, I., Rayner, P. J., Bousquet, P., Fortems-Cheiney, A., and Chevallier, F.: Can we detect regional methane anomalies? A comparison between three observing systems, Atmos. Chem. Phys., 16, 9089-9108, doi:10.5194/acp-16-9089-2016, 2016.

Crevoisier, C., Sweeney, C., Gloor, M., Sarmiento, J. L., and Tans, P. P.: Regional U.S. carbon sinks from three-dimensional atmospheric CO_2 sampling, *Proc. Natl. Acad. Sci.* (2010), 107: 18348-18353, 2010.

Crowell, S., Baker, D., Schuh, A., Basu, S., Jacobson, A. R., Chevallier, F., Liu, J., Deng, F., Feng, L., McKain, K., Chatterjee, A., Miller, J. B., Stephens, B. B., Eldering, A., Crisp, D., Schimel, D., Nassar, R., O'Dell, C. W., Oda, T., Sweeney, C., Palmer, P. I., and Jones, D. B. A.: The 2015–2016 carbon cycle as seen from OCO-2 and the global in situ network, Atmos. Chem. Phys., 19, 9797–9831, https://doi.org/10.5194/acp-19-9797-2019, 2019.

Dee, D. P., et al., The ERA-Interim reanalysis: configuration and performance of the data assimilation system, Q. J. R. Meteorol. Soc., 137, 553–597, 2011.

Desroziers G., Berre, L., Chapnik, B., and Poli, P.: Diagnosis of observation, background and analysis error statistics in observation space. *Q. J. Roy. Meteor. Soc*., 131, 3385-3396, 2005.

Detmers, R., Hasekamp, O., Aben, I., Houweling, S., van Leeuwen, T.T., Butz, A., Landgraf, J., Kohler, P., Guanter, L., and Poulter, B.: Anomalous carbon uptake in Australia as seen by GOSAT. *Geophysical Research Letters*, 42(19), 2015

Dlugokencky, E. J., L. P. Steele, P. M. Lang, and K. A. Masarie, The growth rate and distribution of atmospheric methane, *J. Geophys. Res*., 99, 17021–17043. 1994.

Dlugokencky, E. J., S. Houweling, L. Bruhwiler, K. A. Masarie, P.M. Lang, J. B. Miller, and P. P. Tans, Atmospheric methane levels off: Temporary pause or a new steady-state? *Geophys. Res. Lett*., 30(19), 1992, doi:10.1029/2003GL018126, 2003.

Dlugokencky, E. J., Bruhwiler, L., White, J. W. C., et al., Observational constraints on recent increases in the atmospheric CH_4 burden, *Geophys. Res. Lett.*, 36, L18803, doi:10.1029/2009GL039780, 2009.

Dlugokencky, E., P. Lang, J. Mund, A. Crotwell, M. Crotwell, and K. Thoning, Atmospheric carbon dioxide dry air mole fractions from the NOAA ESRL carbon cycle cooperative global air sampling network, 1968-2015, 2016.

Dubovik, O. and King, M. D.: A flexible inversion algorithm for retrieval of aerosol optical properties from Sun and sky radiance measurements, *J. Geophys. Res*., 105, 20673–20696, 2000.

Enting, I. G.: Inverse Problems in Atmospheric Constituent Transport. Cambridge University Press, 2002.

ESA: A-SCOPE - Advanced Space Carbon and Climate Observation of Planet Earth, Technical Report SP-1313/1, European Space Agency, Noordwijk, The Netherlands. 2008

Feng, L., Palmer, P. I., Bösch, H., and Dance, S.: Estimating surface CO_2 fluxes from space-borne CO_2 dry air mole fraction observations using an ensemble Kalman Filter, *Atmos. Chem. Phys*., 9, 2619–2633, doi:10.5194/acp-9-2619-2009, 2009.

Feng, L., P. I. Palmer, R. J. Parker, et al., Estimates of European uptake of CO_2 inferred from GOSAT X_{CO2} retrievals: sensitivity to measurement bias inside and outside Europe, *Atmos. Chem. Phys*., 16, 1289-1302, doi:10.5194/acp-16-1289-2016, 2016a.

Feng, L., Palmer, P. I., Bösch, H., Parker, R. J., Webb, A. J., Correia, C. S. C., Deutscher, N. M., Domingues, L. G., Feist, D. G., Gatti, L. V., Gloor, E., Hase, F., Kivi, R., Liu, Y., Miller, J. B., Morino, I., Sussmann, R., Strong, K., Uchino, O., Wang, J., and Zahn, A.: Consistent regional fluxes of CH4 and CO2 inferred from GOSAT proxy XCH4:XCO2 retrievals, 2010–2014, Atmos. Chem. Phys. Discuss., doi:10.5194/acp-2016-868, in review, 2016b.Frankenberg, C., Aben, I., Bergamaschi, P., et al., Global column-averaged methane mixing ratios from 2003 to 2009 as derived from SCIAMACHY: Trends and variability, *J. Geophys. Res*., doi:10.1029/2010JD014849, 2011.

Frankenberg, C., Product User Guide (PUG) for the IMAP-DOAS XCH4 SCIAMACHY Data Products, version 1, ESA Climate Change Initiative (CCI) GHG-CCI project, 13 Dec. 2012, 2012.

Fraser, A., Palmer, P. I., Feng, L., et al., Estimating regional methane surface fluxes: the relative importance of surface and GOSAT mole fraction measurements, *Atmos. Chem. Phys*., 13, 5697-5713, doi:10.5194/acp-13-5697-2013, 2013.

Fraser, A., Palmer, P. I., Feng, L. et al., Estimating regional fluxes of CO_2 and CH_4 using space-borne observations of XCH_4:XCO_2, *Atmos. Chem. Phys.*, 14, 12883-12895, doi:10.5194/acp-14-12883-2014, 2014.

Friedl, M. A., Strahler, A. H., and Hodges, J.: ISLSCP II MODIS (Collection 4) IGBP Land Cover, 2000–2001, in: ISLSCP Initia- tive II Collection, Data set, edited by: Hall, F. G., Collatz, G., Meeson, B., Los, S., Brown de Colstoun, E., and Landis, D., Oak Ridge National Laboratory Distributed Active Archive Center, Oak Ridge, Tennessee, USA, doi:10.3334/ORNLDAAC/96

Gatti, L. V., Gloor, M., Miller, J. B., Doughty, C. E., Malhi, Y., Domingues, L. G., Basso, L. S., Martinewski, A., Correia, C. S. C., Borges, V. F., Freitas, S., Braz, R., Anderson, L. O., Rocha, H., Grace, J., Philips, O. L., and Lloyd, J.: Drought sensitivity of Amazonian carbon balance revealed by atmospheric measurements, *Nature*, 506(7486), 76-80, doi:10.1038/nature12957, 2014

Cooperative Global Atmospheric Data Integration Project. (2020). *Multi-laboratory compilation of atmospheric carbon dioxide data for the period 1957-2019; obspack_co2_1_GLOBALVIEWplus_v6.0_2020_09_11* [Data set]. NOAA Earth System Research Laboratory, Global Monitoring Division. https://doi.org/10.25925/20200903

Guerlet, S., Basu, S., Butz, A., et al., Reduced carbon uptake during the 2010 Northern Hemisphere summer from GOSAT, *Geophys. Res. Lett.*, doi: 10.1002/grl.50402, 2013.

Gurney, K.R., et al.: Towards robust regional estimates of CO_2 sources and sinks using atmospheric transport models. *Nature*, 415:6872, 626-630, 2002.

Harris, I., Jones, P.D., Osborn, T.J. and Lister, D.H., Updated high-resolution grids of monthly climatic observations – the CRU TS3.10 Dataset. *Int. J. Climatol*. doi: 10.1002/joc.3711, 2013

Haverd, V., Raupach, M. R., Briggs, P. R., J. G. Canadell., Davis, S. J., Law, R. M., Meyer, C. P., Peters, G. P., Pickett-Heaps, C., and Sherman, B.: The Australian terrestrial carbon budget, *Biogeosciences*, 10, 851-869, doi:10.5194/bg-10-851-2013, 2013.

Hayman, G. D., O'Connor, F. M., Dalvi, et al., Comparison of the HadGEM2 climate-chemistry model against in-situ and SCIAMACHY atmospheric methane data, *Atmos. Chem. Phys*., 14, 13257-13280, doi:10.5194/acp-14-13257-2014, 2014.

Heimann, M.: The global atmospheric tracer model TM2, Technical Report No. 10, Max-Planck-Institut für Meteorologie, Hamburg, Germany. 1995

Heimann, M., G. Esser, A. Haxeltine, J. Kaduk, D.W. Kicklighter, W. Knorr, G. H. Kohlmaier, A. D. McGuire, J. Melillo, B. Moore, et al., Evaluation of terrestrial carbon cycle models through simulations of the seasonal cycle of atmospheric CO2: First results of a model intercomparison study, Global Biogeochemical Cycles, 12, 1–24, 1998.

Heimann, M. and S. Körner: The global atmospheric tracer model TM3. In: Max-Planck-Institut für Biogeochemie (Eds.): Technical Report. Vol. 5. Max-Planck-Institut für Biogeochemie, Jena. pp. 131, 2003.

Heymann, J., Schneising, O., Reuter, M., et al., SCIAMACHY WFM-DOAS XCO_2: comparison with CarbonTracker XCO_2 focusing on aerosols and thin clouds, *Atmos. Meas. Tech.*, 5, 1935-1952, 2012.

Hourdin, F., Foujols, M.-A., Codron, F., Guemas, V., Dufresne, J.-L., Bony, S., Denvil, S., Guez, L., Lott, F., Ghattas, J., Braconnot, P., Marti, O., Meurdesoif, Y., & Bopp, L. (2013). Impact of the LMDZ atmospheric grid configuration on the climate and sensitivity of the IPSL-CM5A coupled model. Climate Dynamics, 40, 2167–2192. https://doi.org/10.1007/s00382-012-1411-3

Houweling, S., et al.: The importance of transport model uncertainties for the estimation of CO_2 sources and sinks using satellite measurements. *Atmos. Chem. Phys*., 10, 9981-9992, doi:10.5194/acp-10-9981-2010, 2010.

Houweling, S., M. Krol, P. Bergamaschi, C. Frankenberg, E. J. Dlugokencky, I. Morino, J. Notholt, V. Sherlock, D. Wunch, V. Beck, C. Gerbig, H. Chen, E. A. Kort, T. Röckmann and I. Aben, A multi-year methane inversion using SCIAMACHY, accounting for systematic errors using TCCON measurements, *Atmos. Chem. Phys*., 14, 3991–4012, doi:10.5194/acp-14-3991-2014, 2014.

Houweling, S., D. Baker, S. Basu, H. Boesch, A. Butz, F. Chevallier, F. Deng, E. Dlugockencky, L. Feng, A. Ganshin, O. P. Hasekamp, D. Jones, S. Maksyutov, J. Marshall, T. Oda, C. O'Dell, S. Oshchepkov, P. Paul, P. Peylin, Z. Poussi, F. Reum, H. Takagi, Y. Yoshida, R. Zhuravlev, An inter-comparison of inverse models for estimating sources and sinks of CO_2 using GOSAT measurements. *J. Geophys. Res. Atmos*., 120, 5253–5266, doi:10.1002/2014JD022962, 2015.

Hu, H., Hasekamp, O., Butz, A., Galli, A., Landgraf, J., Aan de Brugh, J., Borsdorff, T., Scheepmaker, R., and Aben, I.: The operational methane retrieval algorithm for TROPOMI, Atmos. Meas. Tech., 9, 5423–5440, https://doi.org/10.5194/amt-9-5423-2016, 2016.

Kirschke, S., Bousquet, P., Ciais, P., et al., Three decades of global methane sources and sinks, *Nat. Geosci*., 6, 813–823, doi:10.1038/ngeo1955, 2013.

Kort, E. A., Frankenberg, C., Costigan, K. R., et al., Four corners: The largest US methane anomaly viewed from space, *Geophys. Res. Lett*., 41, doi:10.1002/2014GL061503, 2014.

Krol, M. C., S. Houweling, B. Bregman, M. van den Broek, A. Segers, P. van Velthoven, W. Peters, F. Dentener, and P. Bergamaschi, The two-way nested global chemistry-transport zoom model TM5: algorithm and applications, *Atmos. Chem. Phys*., 5, 417-432, 2005.

Lindqvist, H., C. W. O'Dell, S. Basu, H. Boesch, F. Chevallier, N. Deutscher, L. Feng, B. Fisher, F. Hase, M. Inoue, R. Kivi, I. Morino, P. I. Palmer, R. Parker, M. Schneider, R. Sussmann, and Y. Yoshida, Does GOSAT capture the true seasonal cycle of carbon dioxide?; *Atmos. Chem. Phys*., 15, 13023-13040, doi:10.5194/acp-15-13023-2015, 2015.

Lorente, A., Borsdorff, T., Butz, A., Hasekamp, O., aan de Brugh, J., Schneider, A., Wu, L., Hase, F., Kivi, R., Wunch, D., Pollard, D. F., Shiomi, K., Deutscher, N. M., Velazco, V. A., Roehl, C. M., Wennberg, P. O., Warneke, T., and Landgraf, J.: Methane retrieved from TROPOMI: improvement of the data product and validation of the first 2 years of measurements, Atmos. Meas. Tech., 14, 665–684, https://doi.org/10.5194/amt-14-665-2021, 2021.

Ma, X., A. Huete, J. Cleverly, D. Eamus, F. Chevallier, J. Joiner, B. Poulter, Y. Zhang, L. Guanter, W. Meyer, Z. Xie, G. Ponce-Campos: Drought rapidly disseminates the 2011 large CO_2 uptake in semi-arid Australia. Scientific Reports, 6. doi: 10.1038/srep37747, 2016.

Mäder, J. A., J. Staehelin, D. Brunner, W. A. Stahel, I. Wohltmann, and T. Peter, Statistical modeling of total ozone: Selection of appropriate explanatory variables, *J. Geophys. Res*., 112, D11108, doi:10.1029/2006JD007694, 2007.

Meirink, J. F., P. Bergamaschi, and M. Krol: Four-dimensional variational data assimilation for inverse modelling of atmospheric methane emissions: Method and comparison with synthesis inversion, *Atmos. Chem. Phys*., 8, 6341–6353, 2008.

Monteil, G., Houweling, S., Butz, A., et al., Comparison of CH_4 inversions based on 15 months of GOSAT and SCIAMACHY observations, *J. Geophy. Res.*, doi: 10.1002/2013JD019760, Vol 118, Issue 20, 11807-11823, 2013.

O'Dell, C. W., Connor, B., Bösch, H., O'Brien, D., Frankenberg, C., Castano, R., Christi, M., Eldering, D., Fisher, B., Gunson, M., McDuffie, J., Miller, C. E., Natraj, V., Oyafuso, F., Polonsky, I., Smyth, M., Taylor, T., Toon, G. C., Wennberg, P. O., and Wunch, D.: The ACOS CO2 retrieval algorithm – Part 1: Description and validation against synthetic observations, *Atmos. Meas. Tech*., 5, 99–121, doi:10.5194/amt-5-99-2012, 2012.

O'Dell, C. W., Eldering, A., Wennberg, P. O., Crisp, D., Gunson, M. R., Fisher, B., Frankenberg, C., Kiel, M., Lindqvist, H., Mandrake, L., Merrelli, A., Natraj, V., Nelson, R. R., Osterman, G. B., Payne, V. H., Taylor, T. E., Wunch, D., Drouin, B. J., Oyafuso, F., Chang, A., McDuffie, J., Smyth, M., Baker, D. F., Basu, S., Chevallier, F., Crowell, S. M. R., Feng, L., Palmer, P. I., Dubey, M., García, O. E., Griffith, D. W. T., Hase, F., Iraci, L. T., Kivi, R., Morino, I., Notholt, J., Ohyama, H., Petri, C., Roehl, C. M., Sha, M. K., Strong, K., Sussmann, R., Te, Y., Uchino, O., and Velazco, V. A.: Improved retrievals of carbon dioxide from Orbiting Carbon Observatory-2 with the version 8 ACOS algorithm, Atmos. Meas. Tech., 11, 6539–6576, https://doi.org/10.5194/amt-11-6539-2018, 2018.

Oda, T., and Maksyutov, S.: A very high-resolution (1 km×1 km) global fossil fuel CO2 emission inventory derived using a point source database and satellite observations of nighttime lights, *Atmos. Chem. Phys*., 11, 543–556, doi:10.5194/acp-11-543-2011, 2011.

Olivier, J. G. J., van Aardenne, J. A., Dentener, F., Ganzeveld, L., and Peters, J. A. H. W.: Recent trends in global greenhouse gas emissions: regional trends and spatial distribution of key sources, in: Non-CO2 Greenhouse Gases (NCGG-4), edited by: van Amstel, A., Millpress, Rotterdam, 325–330, 2005.

Olivier, J. G. J., Janssens-Maenhout, G., and Peters, J. A. H. W., Trends in global CO_2 emissions, 2012 Report, PBL Netherlands Environmental Assessment Agency, The Hague, Joint Research Centre, Ispra, ISBN 978-92-79-25381-2, 2012.

Oshchepkov, S., A. Bril, T. Yokota, et al., Effects of atmospheric light scattering on spectroscopic observations of greenhouse gases from space. Part 2: Algorithm intercomparison in the GOSAT data processing for CO_2 retrievals over TCCON sites, *J. Geophys. Res.*, 118, 1493–1512, doi:10.1002/jgrd.50146, 2013.

Osterman, G., O'Dell, C., Eldering, A., Fisher, B., Crisp, D., Cheng, C., Frankenberg, C., Lambert, A., Gunson, M., Mandrake, L., & Wunch, D. (2020). Orbiting Carbon Observatory-2 & 3(OCO-2 & OCO-3)—Data product user's guide, operational level 2 data versions 10 and lite file version 10 and VEarly.

Version 1.0, revision A, 8 June 2020. Pasadena, CA: Jet Propulsion Laboratory. Retrieved from https://docserver.gesdisc.eosdis.nasa.gov/public/project/OCO/OCO2_OCO3_B10_DUG.pdf

Pandey, S., Houweling, S., Krol, M., Aben, I., Chevallier, F., Dlugokencky, E. J., Gatti, L. V., Gloor, M., Miller, J. B., Detmers, R., Machida, T., and Röckmann, T.: Inverse modeling of GOSAT-retrieved ratios of total column CH_4 and CO_2 for 2009 and 2010, *Atmos. Chem. Phys. Discuss*., doi:10.5194/acp-2016-77, in review, 2016.

Parazoo, N. C., Bowman, K., Frankenberg, C., et al., Interpreting seasonal changes in the carbon balance of southern Amazonia using measurements of XCO_2 and chlorophyll fluorescence from GOSAT, *Geophys. Res. Lett.*, 40, 2829–2833, doi:10.1002/grl.50452, 2013.

Parker, R., Boesch, H., Cogan, A., et al., Methane Observations from the Greenhouse gases Observing SATellite: Comparison to ground-based TCCON data and Model Calculations, *Geophys. Res. Lett*., doi:10.1029/2011GL047871, 2011.

Peters, W., Jacobson, A. R., Sweeney, C., et al.: An atmospheric perspective on North American carbon dioxide exchange: CarbonTracker, *Proceedings of the National Academy of Sciences* (*PNAS*) of the United States of America, 27 Nov. 2007, 104(48), 18925-18930, 2007.

Peylin, P., Law, R. M., Gurney, et al., Global atmospheric carbon budget: results from an ensemble of atmospheric CO_2 inversions, *Biogeosciences*, 10, 6699–6720, doi:10.5194/bg-10-6699-2013, URL http://www.biogeosciences.net/10/6699/2013/, 2013.

Pinty, B., G. Janssens-Maenhout, M. Dowell, H. Zunker, T. Brunhes, P. Ciais, D. Dee, H. Denier van der Gon, H. Dolman, M. Drinkwater, R. Engelen, M. Heimann, K. Holmlund, R. Husband, A. Kentarchos, Y. Meijer, P. Palmer and M. Scholze (2017) An operational anthropogenic CO_2 emissions monitoring & verification support capacity - Baseline requirements, Model components and functional architecture, doi:10.2760/39384, European Commission Joint Research Centre, EUR 28736 EN.

Poulter, B., Frank, D., Ciais, P., Myneni, R. B., Andela, N., Bi, J., Broquet, G. Canadell, J.G. Chevallier, F. Liu, Y. Y., Running, S. W., Sitch, S., and van der Werf, G. R.: Contribution of semi-arid ecosystems to interannual variability of the global carbon cycle. *Nature*, doi:10.1038/nature13376, 2014.

Prather, M.: Interactive comment on "Carbon dioxide and climate impulse response functions for the computation of greenhouse gas metrics: a multi-model analysis" by F. Joos et al, Atmos. Chem. Phys. Discuss., 12, C8465–C8470, www.atmos-chem-phys-discuss.net/12/C8465/2012/, 2012.

Remaud, M., Chevallier, F., Cozic, A., Lin, X., and Bousquet, P.: On the impact of recent developments of the LMDz atmospheric general circulation model on the simulation of CO_2 transport, Geosci. Model Dev., 11, 4489–4513, https://doi.org/10.5194/gmd-11-4489-2018, 2018.

Reuter, M., Bovensmann, H., Buchwitz, M., et al., Retrieval of atmospheric CO_2 with enhanced accuracy and precision from SCIAMACHY: Validation with FTS measurements and comparison with model results, *J. Geophys. Res*., 116, D04301, doi:10.1029/2010JD015047, 2011.

Reuter, M., Boesch, H., Bovensmann, H., et al., A joint effort to deliver satellite retrieved atmospheric CO_2 concentrations for surface flux inversions: the ensemble median algorithm EMMA, *Atmos. Chem. Phys*., 13, 1771-1780, 2013.

Reuter, M., M. Buchwitz, M. Hilker, et al., Satellite-inferred European carbon sink larger than expected, *Atmos. Chem. Phys*., 14, 13739-13753, doi:10.5194/acp-14-13739-2014, 2014a.

Reuter, M., M. Buchwitz, A. Hilboll, et al., Decreasing emissions of NOx relative to CO_2 in East Asia inferred from satellite observations, *Nature Geoscience*, 28 Sept. 2014, doi:10.1038/ngeo2257, pp.4, 2014b.

Reuter, M.: ESA Climate Change Initiative (CCI) Product User Guide version 4 (PUGv4) for the XCO2 SCIAMACHY Data Product BESD for the Essential Climate Variable (ECV): Greenhouse Gases (GHG), 31 August 2016, 2016a.

Reuter, M., M. Hilker, O. Schneising, M. Buchwitz, J. Heymann ESA Climate Change Initiative (CCI) Comprehensive Error Characterisation Report: BESD full-physics retrieval algorithm for XCO_2 for the Essential Climate Variable (ECV) Greenhouse Gases (GHG) Version 2.0, revision 1. 2016b.

Reuter, M., M. Buchwitz, M. Hilker, J. Heymann, H. Bovensmann, J. P. Burrows, S. Houweling, Y. Y. Liu, R. Nassar, F. Chevallier, et al., How much CO_2 is taken up by the European terrestrial biosphere?, Bulletin of the AmericanMeteorological Society, 0(0), doi:10.1175/BAMS-D-15-00310.1, 2016c.

Reuter, M., M. Buchwitz, O. Schneising, S. Noel, V. Rozanov, H. Bovensmann, J. P. Burrows, A Fast Atmospheric Trace Gas Retrieval for Hyperspectral Instruments Approximating Multiple Scattering - Part 1: Radiative Transfer and a Potential OCO-2 XCO_2 Retrieval Setup, Remote Sens., 9, 1159, doi:10.3390/rs9111159, 2017a.

Reuter, M., M. Buchwitz, O. Schneising, S. Noel, H. Bovensmann, J. P. Burrows, A Fast Atmospheric Trace Gas Retrieval for Hyperspectral Instruments Approximating Multiple Scattering - Part 2: Application to XCO_2 Retrievals from OCO-2, Remote Sens., 9, 1102, doi:10.3390/rs9111102, 2017b.

Reuter, M., Buchwitz, M., Schneising, O., Noël, S., Bovensmann, H., Burrows, J. P., Boesch, H., Di Noia, A., Anand, J., Parker, R. J., Somkuti, P., Wu, L., Hasekamp, O. P., Aben, I., Kuze, A., Suto, H., Shiomi, K., Yoshida, Y., Morino, I., Crisp, D., O'Dell, C. W., Notholt, J., Petri, C., Warneke, T., Velazco, V. A., Deutscher, N. M., Griffith, D. W. T., Kivi, R., Pollard, D. F., Hase, F., Sussmann, R., Té, Y. V., Strong, K., Roche, S., Sha, M. K., De Mazière, M., Feist, D. G., Iraci, L. T., Roehl, C. M., Retscher, C., and Schepers, D.: Ensemble-based satellite-derived carbon dioxide and methane column-averaged dry-air mole fraction data sets (2003–2018) for carbon and climate applications, Atmos. Meas. Tech., 13, 789–819, https://doi.org/10.5194/amt-13-789-2020, 2020.

Rödenbeck, C.: Estimating CO_2 sources and sinks from atmospheric mixing ratio measurements using a global inversion of atmospheric transport, Tech. Rep. 6, Max Planck Institute for Biogeochemistry, Jena, Germany, 2005.

Ross, A. N., Wooster, M. J., Boesch, H., Parker, R., First satellite measurements of carbon dioxide and methane emission ratios in wildfire plumes, *Geophys. Res. Lett.*, 40, 1-5, doi:10.1002/grl.50733, 2013.

Scarcle, J. D., Studies in astronomical time series analysis. III. Fourier transforms, autocorrelation functions and cross-correlation functions of unevenly spaced data. *Astrophys. J.*, 343, 874–887, 1989.

Schneising, O., Buchwitz, M., Reuter, M., et al., Long-term analysis of carbon dioxide and methane column-averaged mole fractions retrieved from SCIAMACHY, *Atmos. Chem. Phys*., 11, 2881-2892, 2011.

Schneising, O., J. Heymann, M. Buchwitz, M. Reuter, H. Bovensmann, and J. P. Burrows, Anthropogenic carbon dioxide source areas observed from space: assessment of regional enhancements and trends, *Atmos. Chem. Phys*., 13, 2445-2454, 2013.

Schneising, O., M. Reuter, M. Buchwitz, J. Heymann, H. Bovensmann, and J. P. Burrows, Terrestrial carbon sink observed from space: variation of growth rates and seasonal cycle amplitudes in response to interannual surface temperature variability, *Atmos. Chem. Phys*., 14, 133-141, 2014a.

Schneising, O., J. P. Burrows, R. R. Dickerson, M. Buchwitz, M. Reuter, H. Bovensmann, Remote sensing of fugitive methane emissions from oil and gas production in North American tight geologic formations, *Earth's Future*, 2, DOI: 10.1002/2014EF000265, pp. 11, 2014b.

Schneising, O., Buchwitz, M., Reuter, M., Bovensmann, H., Burrows, J. P., Borsdorff, T., Deutscher, N. M., Feist, D. G., Griffith, D. W. T., Hase, F., Hermans, C., Iraci, L. T., Kivi, R., Landgraf, J., Morino, I., Notholt, J., Petri, C., Pollard, D. F., Roche, S., Shiomi, K., Strong, K., Sussmann, R., Velazco, V. A., Warneke, T., and Wunch, D.: A scientific algorithm to simultaneously retrieve carbon monoxide and methane from TROPOMI onboard Sentinel-5 Precursor, Atmos. Meas. Tech., 12, 6771–6802, https://doi.org/10.5194/amt-12-6771-2019, 2019.

Schulze, E. D., Luyssaert, S., Ciais, P., Freibauer, A., Janssens, I. A., Soussana, J. F., Smith, P., Grace, J., Levin, I., Tiruchittampalam, B., Heimann, M., Dolman, A. J., Valentini, R., Bousquet, P., Peylin, P., Peters, W., Rodenbeck, C., Etiope, G., Vuichard, N., Wattenbach, M., Nabuurs, G. J., Poussi, Z., Nieschulze, J., Gash, J. H., and Team, C.: Importance of methane and nitrous oxide emissions for europe's terrestrial greenhouse gas balance, *Nat. Geosci*., 2, 842–850, 2009.

Shindell, D. T., O. Pechony, A. Voulgarakis, et al., Interactive ozone and methane chemistry in GISS-E2 historical and future climate simulations, *Atmos. Chem. Phys.*, 13, 2653–2689, doi:10.5194/acp-13-2653-2013, 2013.

Somkuti, P.: ESA Climate Change Initiative (CCI) Product User Guide version 4.0 (PUGv4.0) for the University of Leicester full-physics XCO_2 GOSAT data product (CO2_GOS_OCFP version 7) for the Essential Climate Variable (ECV): Greenhouse Gases (GHG), 31 August 2016, 2016.

Sussmann, R., Forster, F., Rettinger, M., and Bousquet, P.: Renewed methane increase for five years (2007–2011) observed by solar FTIR spectrometry, Atmos. Chem. Phys., 12, 4885-4891, doi:10.5194/acp-12-4885-2012, 2012.

Turner, A. J., Jacob, D. J., Wecht, K. J., Maasakkers, J. D., Lundgren, E., Andrews, A. E., Biraud, S. C., Boesch, H., Bowman, K. W., Deutscher, N. M., Dubey, M. K., Griffith, D. W. T., Hase, F., Kuze, A., Notholt, J., Ohyama, H., Parker, R., Payne, V. H., Sussmann, R., Sweeney, C., Velazco, V. A., Warneke, T., Wennberg, P. O., and Wunch, D.: Estimating global and North American methane emissions with high spatial resolution using GOSAT satellite data, *Atmos. Chem. Phys*., 15, 7049-7069, doi:10.5194/acp-15-7049-2015, 2015.

Wanninkhof, R., Park, G. -H., Takahashi, T., Sweeney, C., Feely, R., Nojiri, Y., Gruber, N., Doney, S. C., McKinley, G. A., Lenton, A., Le Quéré, C., Heinze, C., Schwinger, J., Graven, H., and Khatiwala, S.: Global ocean carbon uptake: magnitude, variability and trends, *Biogeosciences*, 10, 1983-2000, doi:10.5194/bg-10-1983-2013, 2013.

van der Werf, G. R., Randerson, J. T., Giglio, L., Collatz, G. J., Mu, M., Kasibhatla, P. S., Morton, D. C., DeFries, R. S., Jin, Y., and van Leeuwen, T. T.: Global fire emissions and the contribution of deforestation, savanna, forest, agricultural, and peat fires (1997–2009), *Atmos. Chem. Phys*., 10, 11707-11735, doi:10.5194/acp-10-11707-2010, 2010.

Wecht, K. J., D. J. Jacob, C. Frankenberg, Z. Jiang, and D. R. Blake (2014), Mapping of North American methane emissions with high spatial resolution by inversion of SCIAMACHY satellite data, J. Geophys. Res. Atmos., 119, 7741–7756, doi:10.1002/2014JD021551.

Wunch, D., Toon, G. C., Blavier, J.-F., et al., The Total Carbon Column Observing Network, *Phil. Trans. R. Soc. A*, 369, 2087–2112, doi:10.1098/rsta.2010.0240, 2011.

Wunch, D., Wennberg, P. O., Toon, G. C. et al., A method for evaluating bias in global measurements of CO_2 total columns from space. Atmos. Chem. Phys., 11, 12317-12337, 2011.

York, D., Evensen, N., Martinez, M., and Delgado, J.: Unified equations for the slope, intercept, and standard errors of the best straight line. *Am. J. Phys*., 72(3), 367–375, 2004.

Yoshida, Y., Kikuchi, N., Morino, I., et al., Improvement of the retrieval algorithm for GOSAT SWIR XCO_2 and XCH_4 and their validation using TCCON data, *Atmos. Meas. Tech*., 6, 1533–1547, doi:10.5194/amt-6-1533-2013, 2013.

END OF DOCUMENT